Chapter 4

Enzymology

4.1. Introduction

In this chapter selected drugs that were found to map to the structure-based pharmacophore models of MAO-A and MAO-B will be evaluated as *in vitro* inhibitors of the MAO enzymes. Not all of the hits will be evaluated as *in vitro* inhibitors and only a subset will be selected for screening. The selection of the compounds to be screened will be based on the commercial availability of the compounds and cost. Drugs that are not readily commercially available and of high cost will not be evaluated. Of the 24 compounds that mapped to the MAO-A pharmacophore, 13 will be evaluated as *in vitro* inhibitors of MAO-A and MAO-B. Of the 21 compounds that mapped to the MAO-B pharmacophore, 13 will be evaluated as *in vitro* inhibitors of MAO-A and MAO-B. The following *in vitro* bioassays will be carried out in this chapter:

- Determination of the IC_{50} values for the inhibition of MAO-A and MAO-B. For this purpose sigmoidal concentration-inhibition curves will be constructed. These experiments will be conducted for *all test drugs*.

- The reversibility of the inhibition of MAO-A and MAO-B by *one selected inhibitor* (esomeprazole) will be examined. For this purpose the recovery of enzyme activity after dilution of the enzyme-inhibitor complexes will be evaluated.

- *For two selected inhibitors* (esomeprazole and caffeine) the reversibility of the inhibition of MAO-A and MAO-B will also be examined by dialysis of enzyme-inhibitor complexes.

- To determine if the active inhibitors are competitive inhibitors, Lineweaver-Burk plots will be constructed. These studies will be conducted *for two selected inhibitors*, esomeprazole and caffeine.

In addition, for those drugs that proved to be particularly interesting inhibitors of MAO-A and/or MAO-B, the docked orientations in MAO-A and/or MAO-B will be presented and their interactions with the active sites of the enzymes will be analyzed. The drugs selected for this purpose are esomeprazole, caffeine and leflunomide. The orientations of these drugs within the structure-based pharmacophore models will also be presented.

In this chapter the methods that were used will firstly be discussed. This will be followed by the results (dose-response curves) for those drugs that mapped to the structure-based pharmacophore models of MAO-A and MAO-B, but proved not to be inhibitors of MAO-A or MAO-B. The results (dose-response curves and results of dilution studies) of those drugs that were found to be MAO-A or MAO-B inhibitors will subsequently be given. As mentioned above for selected inhibitors, the results of the dialysis studies and Lineweaver-Burk plots will also be presented. This chapter will also evaluate and report the MAO-A and MAO-B inhibitory properties of known MAO inhibitors for comparison with the potencies of the drugs that were found to be MAO-A or MAO-B inhibitors. The known inhibitors selected for this purpose are:

- Toloxatone, a reversible MAO-A inhibitor
- Lazabemide, a reversible MAO-B inhibitor

The subsequent chapters (Chapters 5-6) will be presented as two articles, each discussing the MAO inhibitory properties of a selected drug that was found in this study to be a MAO-A and/or MAO-B inhibitor. The purpose of these articles is to evaluate the probability of these drugs to exhibit MAO inhibition in the clinical setting. In addition, the articles will also demonstrate that the results of this study are publishable. Based on their promising or interesting MAO inhibitory potencies, the MAO inhibitory properties of the following drugs will be presented as articles:

- Esomeprazole
- Caffeine

It should be noted that for esomeprazole and caffeine, the MAO inhibition data will be presented in this Chapter as well as in the subsequent articles. Although this will result in some redundancy, this method of presentation will facilitate the detailed discussion of the inhibition data in the articles and prevent ambiguity.

4.2. Enzymology

The inhibition studies with MAO-A and MAO-B were conducted using kynuramine as substrate. Kynuramine displays similar K_m values towards the two enzymes with values of 16.1 and 22.7 µM for MAO-A and MAO-B, respectively (Legoabe *et al*., 2011). The MAO-catalyzed oxidation of kynuramine yields 4-hydroxyquinoline, a fluorescent compound which is readily measured in basic solutions at excitation and emission wavelengths of 310 nm and 400 nm, respectively. Inhibitors may be classified as reversible or irreversible inhibitors. As mentioned above, to evaluate the reversibility of enzyme inhibition, recovery of enzyme activity after dilution of the enzyme-inhibitor complexes will be examined. In select cases dialysis of enzyme-inhibitor complexes will also be performed.

4.3. Materials and methods

The following instruments and chemicals were used in this study:

- A Varian Cary Eclipse fluorescence spectrophotometer was employed for fluorescence spectrophotometry.
- Microsomes from insect cells containing recombinant human MAO-A and MAO-B (5 mg/ml) were obtained from Sigma-Aldrich.
- Kynuramine.2HBr, deprenyl.HCl, pargyline.HCl and 4-hydroxyquinoline were obtained from Sigma-Aldrich.
- The test drugs were obtained from Sigma-Aldrich.

4.3.1. Determination of IC_{50} values

- Microsomal preparations from insect cells containing recombinant human MAO-A and MAO-B (5 mg/ml) served as enzyme sources and all enzymatic reactions were conducted in potassium phosphate buffer (100 mM, pH 7.4, made isotonic with KCl) to a final volume of 500 µl.
- The reactions contained:
    - the MAO mixed substrate, kynuramine, at concentrations of 45 µM and 30 µM for the incubations with MAO-A and MAO-B, respectively,
    - various concentrations of the test inhibitor (0-100 µM),
    - DMSO at a concentration of 4% as co-solvent
    - and the MAO enzymes (0.0075 mg/ml).
- The enzyme reactions were incubated at 37 ˚C for 20 minutes and then terminated with the addition of 400 µl NaOH (2 N) and 1000 µl distilled water.
- After centrifugation at 16,000 g for 10 minutes, the fluorescence of the MAO generated 4-hydroxyquinoline in the supernatant fractions were measured (λ_{ex}=310 nm, λ_{ex}=400 nm).
- To determine the concentration of 4-hydroxyquinoline, a linear calibration curve was constructed from solutions of 4-hydroxyquinoline (0.047–1.50 µM) in potassium phosphate buffer. The calibration standards were prepared to a volume of 500 µl and contained 4% DMSO, 400 µl NaOH (2 N) and 1000 µl distilled water.
- The MAO catalytic rates were calculated from the endpoint concentration of 4-hydroxyquinoline (nM) in the supernatants, the incubation time (20 min) and the enzyme concentration (0.0075 mg protein/mL), and were expressed as nmol 4-hydroxyquinoline formed/min.mg protein.

- The initial rate of MAO catalysis (expressed in %) was plotted versus the logarithm of the inhibitor concentration to obtain a sigmoidal dose-response curve. Each curve was constructed from 6 different inhibitor concentrations spanning at least 3 orders of magnitude. The data were fitted to the one site competition model incorporated into the GraphPad Prism software and IC_{50} values were determined in triplicate and are expressed as mean ± standard deviation.

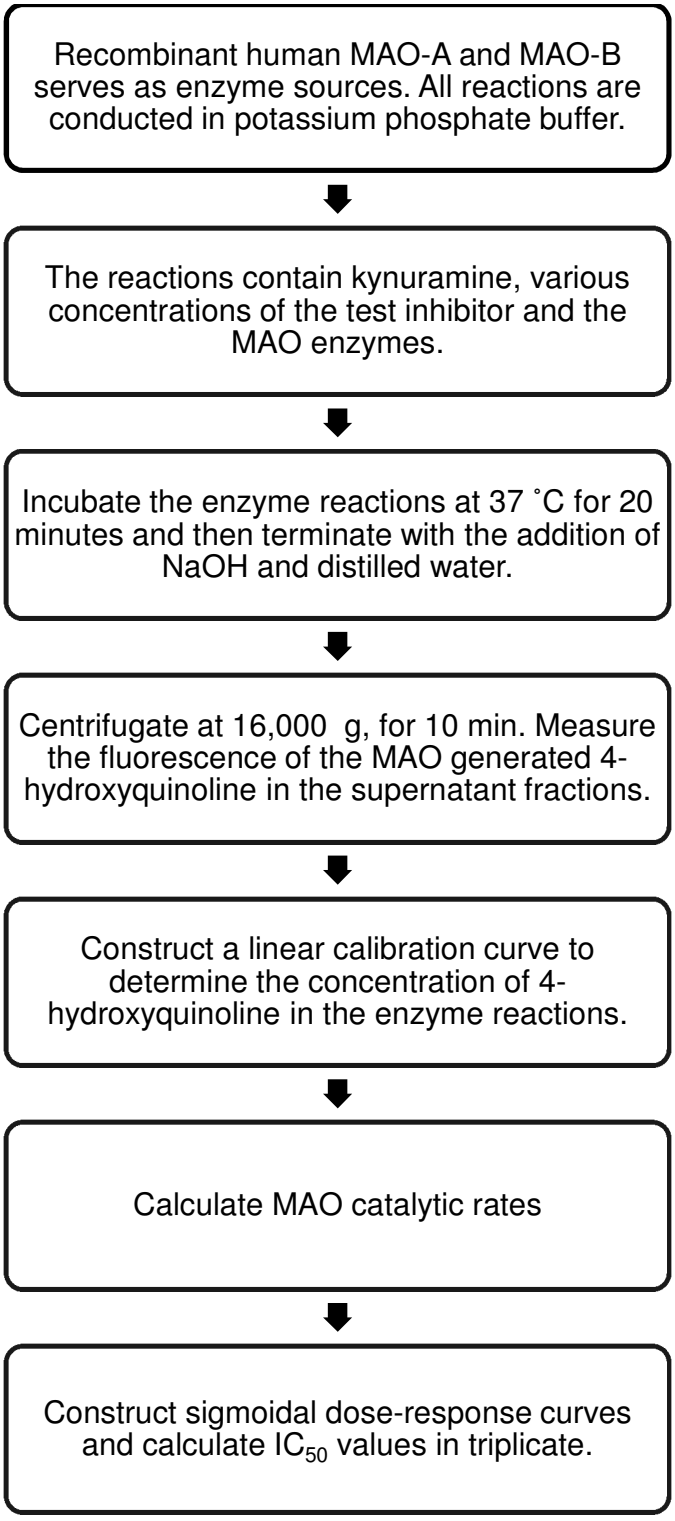

Figure 4.1. Diagrammatic presentation of the protocol followed for the determination of IC_{50} values.

4.3.2. Recovery of enzyme activity after dilution

- The test compound at concentrations equal to 10 x IC_{50} and 100 x IC_{50} was preincubated with recombinant human MAO-A and MAO-B (0.75 mg/ml) for 30 min at 37 ˚C in potassium phosphate buffer (100 mM, pH 7.4, made isotonic with KCl). Control incubations conducted in the absence of the test compound were also included and DMSO (4%) was added as co-solvent to all preincubations.

- These reactions were subsequently diluted 100-fold with the addition of kynuramine to yield final concentrations of the test compound of 0.1 x IC_{50} and 1 x IC_{50}. The final enzyme concentration was 0.0075 mg/ml.

- The reactions were subsequently incubated for a further 20 minutes at 37 ˚C and terminated with the addition of 400 µl NaOH (2 N) and 1000 µl distilled water.

- The residual rates of 4-hydroxyquinoline was determined by constructing a linear calibration curve from solutions of 4-hydroxyquinoline (0.047–1.50 µM) in potassium phosphate buffer. The calibration standards were prepared to a volume of 500 µl and contained 4% DMSO, 400 µl NaOH (2 N) and 1000 µl distilled water.

- These studies were conducted in triplicate and the residual enzyme catalytic rates were expressed as mean ± standard deviation.

- As positive control incubations, pargyline (IC_{50} = 12.97 µM) and (R)-deprenyl (IC_{50} = 0.079 µM) were similarly preincubated with MAO-A and MAO-B, respectively, at 10 × IC_{50} and diluted 100-fold with the addition of kynuramine to yield final concentrations of pargyline and (R)-deprenyl equal to 0.1 × IC_{50} (Petzer *et al.,* 2012).

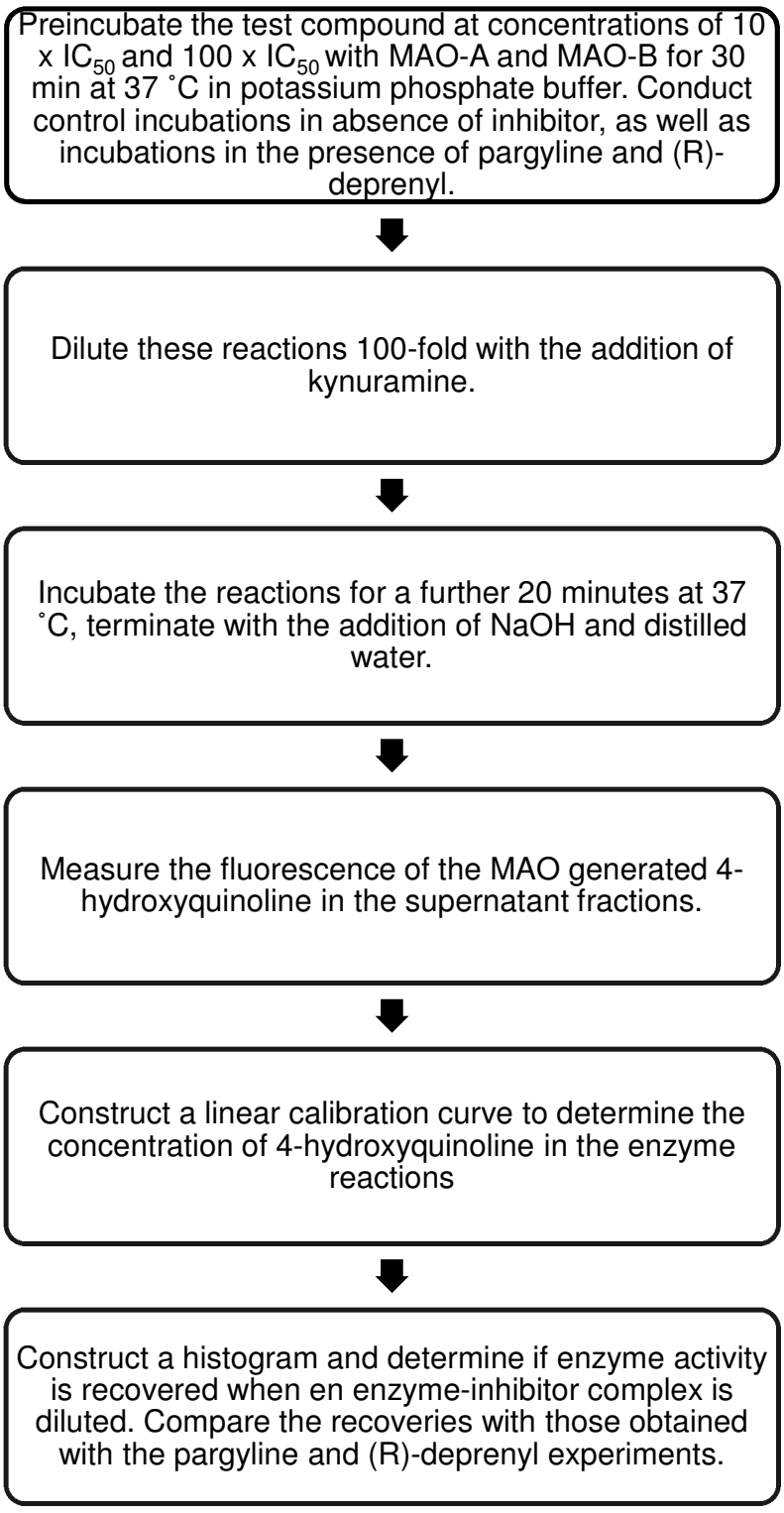

Figure 4.2. Diagrammatic presentation of the protocol followed for the determination of the recovery of enzyme activity after dilution of the enzyme-inhibitor complex.

4.3.3. Dialysis study

- For this study, Slide-A-Lyzer dialysis cassettes (Thermo Scientific), with a molecular weight cut-off of 10 000 and a sample volume capacity of 0.5–3 ml were used.

- The MAO enzymes (0.03 mg/ml) and the test drug, at a concentration equal to fourfold the IC_{50} values for the inhibition of the respective enzymes, were preincubated for 15 min at 37 ℃. These reactions were conducted in potassium phosphate buffer (100 mM, pH 7.4) containing 5% sucrose to final volumes of 0.8 ml. DMSO (4%) was added as co-solvent to all preincubations.

- As controls, MAO-A and MAO-B were similarly preincubated in the absence of inhibitor and presence of the irreversible inhibitors, pargyline and (R)-deprenyl, respectively. The concentrations of pargyline [IC_{50}(MAO-A) = 13 µM] (Strydom *et al.*, 2012) and (R)-deprenyl [IC_{50}(MAO-B) = 0.079 µM] (Petzer *et al.*, 2012) employed were equal to fourfold the IC_{50} values for the inhibition of the respective enzymes.

- The reactions (0.8 ml) were subsequently dialyzed at 4 ℃ in 80 ml of outer buffer (100 mM potassium phosphate, pH 7.4, 5% sucrose). The outer buffer was replaced with fresh buffer at 3 h and 7 h after the start of dialysis.

- At 24 h after dialysis was started, the reactions were diluted twofold with the addition of kynuramine (dissolved in potassium phosphate buffer, 100 mM, pH 7.4, made isotonic with KCl). The final concentration of kynuramine in these reactions was 50 µM while the final inhibitor concentrations were equal to twofold their IC_{50} values for the inhibition of the MAOs.

- The reactions (500 µl) were subsequently incubated for a further 20 minutes at 37 ˚C and terminated with the addition of 400 µl NaOH (2 N) and 1000 µl distilled water.

- The residual rates of 4-hydroxyquinoline was determined by constructing a linear calibration curve from solutions of 4-hydroxyquinoline (0.047–1.50 µM) in potassium phosphate buffer. The calibration standards were prepared to a volume of 500 µl and contained 4% DMSO, 400 µl NaOH (2 N) and 1000 µl distilled water.

- These studies were conducted in triplicate and the residual enzyme catalytic rates were expressed as mean ± standard deviation.

- For comparison, undialyzed mixtures of the MAOs with esomeprazole were maintained at 4 °C over the same time period. All reactions were carried out in triplicate and the residual enzyme catalytic rates were expressed as mean ± SD.

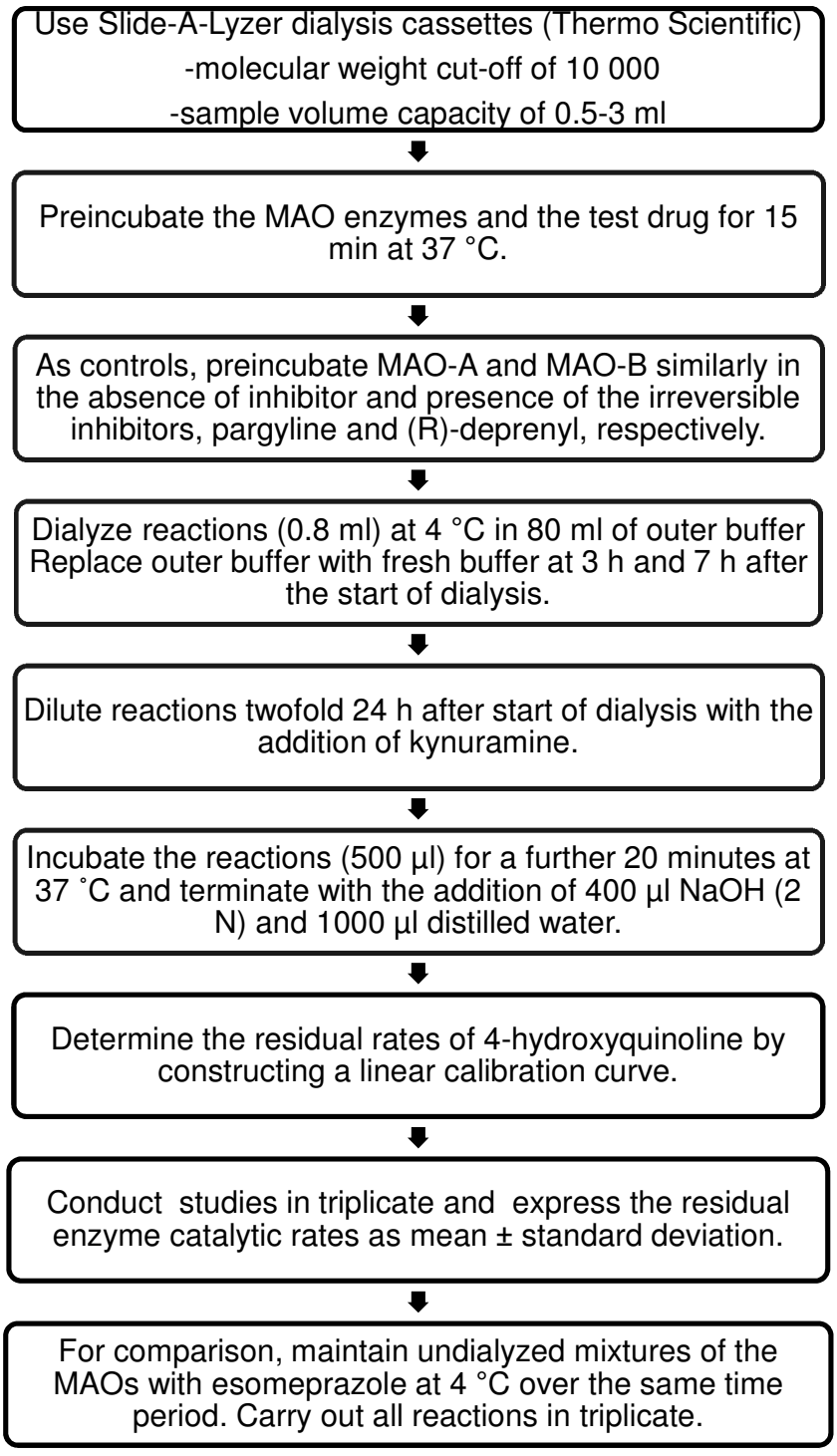

Figure 4.3. Diagrammatic presentation of the protocol followed for the determination of the reversibility of enzyme inhibition by dialysis.

4.3.4. Construction of Lineweaver-Burk plots

- Lineweaver-Burk plots were constructed for the inhibition of MAO-A and MAO-B by measuring the initial rates of kynuramine oxidation at four (for the study with esomeprazole) or eight (for the study with caffeine) different kynuramine concentrations (15–250 µM). These reactions were conducted in the absence and presence of three (for the study with esomeprazole) or five (for the study with caffeine) different concentrations of the test inhibitor. The concentrations of the test compound that were selected were ¼ × IC_{50}, ½ × IC_{50} and 1 × IC_{50} (for the study with esomeprazole) or ¼ × IC_{50}, ½ × IC_{50}, ¾ × IC_{50} , 1 × IC_{50} and 1¼ × IC_{50} (for the study with caffeine).

- The enzyme concentrations in these incubations were 0.015 mg protein/ml.

- The enzyme reactions were incubated at 37 ˚C for 20 minutes and then terminated with the addition of 400 µl NaOH (2 N) and 1000 µl distilled water.

- The residual rates of 4-hydroxyquinoline were determined by constructing a linear calibration curve from solutions of 4-hydroxyquinoline (0.047–1.50 µM) in potassium phosphate buffer.

- The calibration standards were prepared to a volume of 500 µl and contained 4% DMSO, 400 µl NaOH (2 N) and 1000 µl distilled water. Linear regression analysis was performed using GraphPad Prism 5.

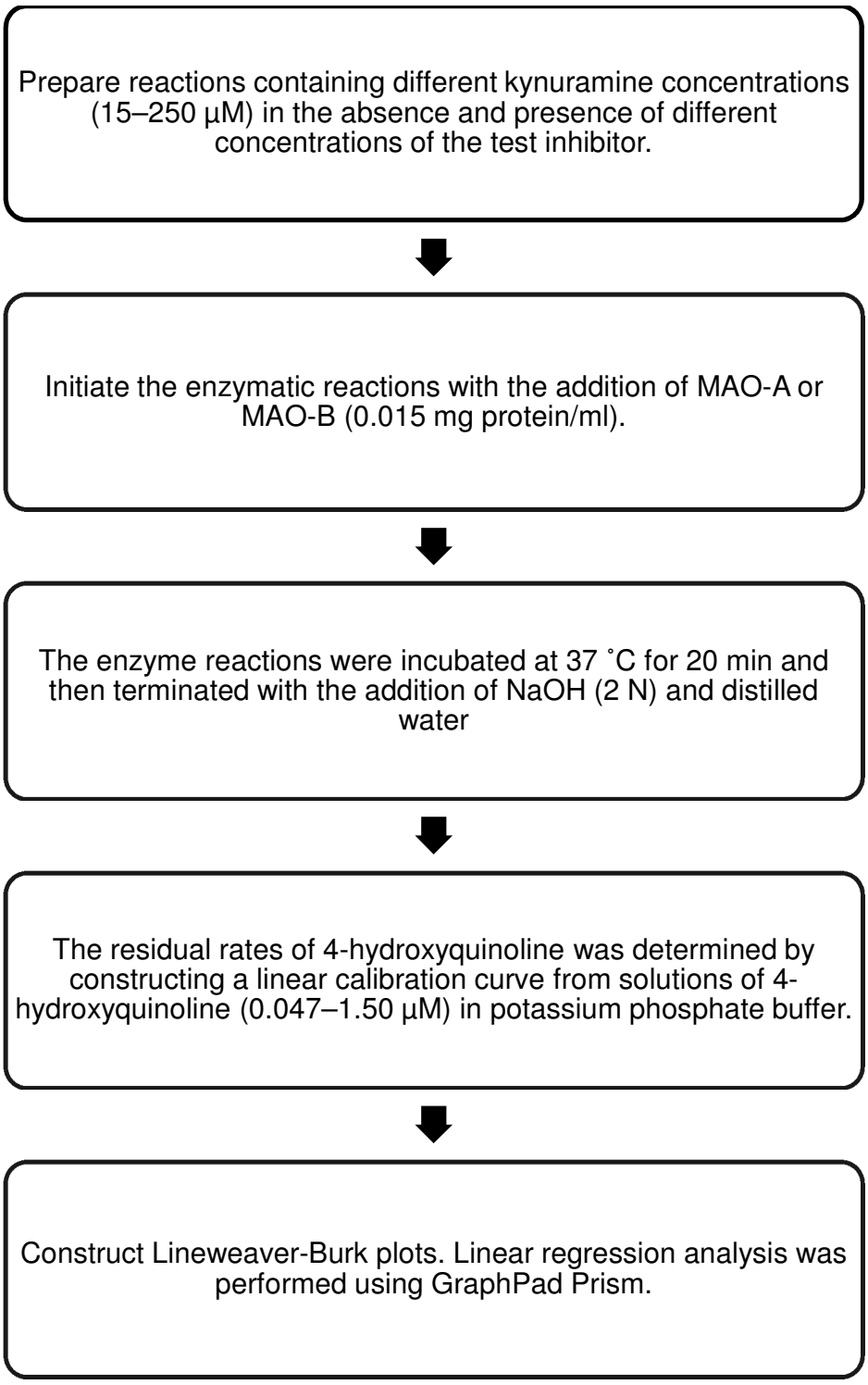

Figure 4.4. Diagrammatic presentation of the protocol followed to construct Lineweaver-Burk plots.

4.3.5. An example of a linear calibration curve.

As mentioned above, linear calibration curves containing 4-hydroxyquinoline (0.047–1.50 µM) were constructed in order to quantify the 4-hydroxyquinoline in the enzymatic reactions. In general, these curves display a high degree of linearity with R^2 values > 0.99. The following is an example of such a calibration curve.

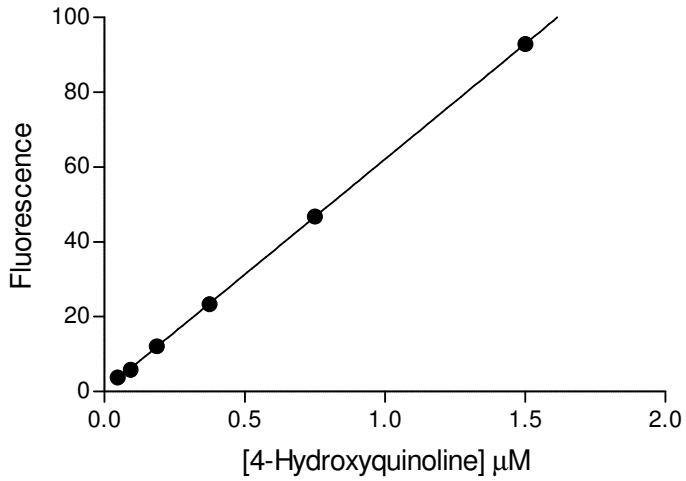

Figure 4.5. Linear calibration curve constructed with 4-hydroxyquinoline (0.047–1.50 µM).

4.4. Results of the MAO inhibition studies with drugs that mapped to the structure-based pharmacophore model of MAO-A and MAO-B, but proved not to be inhibitors *in vitro*.

4.4.1. Acyclovir

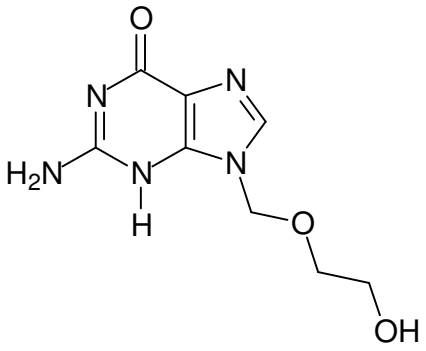

Figure 4.6. The structure of acyclovir.

The structure of acyclovir is given above. Acyclovir is an antiviral nucleoside analogue that exhibits anti-retroviral activity. Acyclovir is phosphorylated by thymidine kinase and subsequently inhibits viral DNA synthesis by competitive inhibition with guanosine triphosphate (Miwa *et al*., 2005). It is used in the treatment of herpes simplex and varicella-zoster virus infections. The results of the MAO inhibition studies show that acyclovir is not an inhibitor of either MAO-A or MAO-B, even at a maximal tested concentration of 100 µM. The concentration-response curves of the MAO-A and MAO-B catalytic activity in presence of increasing concentrations of acyclovir are given below. The graph shows that there is no significant decrease in the catalytic activities of MAO-A and MAO-B with increasing concentrations of acyclovir.

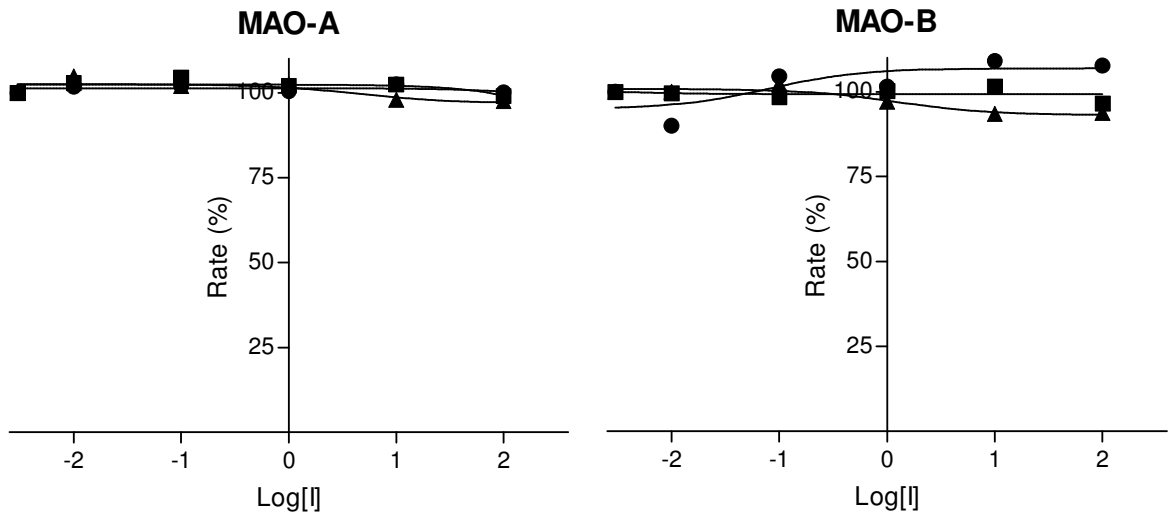

Figure 4.7. The recombinant human MAO-A (left) and MAO-B (right) catalyzed oxidation of kynuramine in the presence of various concentrations of acyclovir (expressed in μM). The concentration-response curves were constructed in triplicate from the initial rates of kynuramine oxidation versus the logarithm of the concentration of acyclovir. The rates are expressed as the percentage of the catalytic rate recorded in the absence of inhibitor.

4.4.2. Atenolol

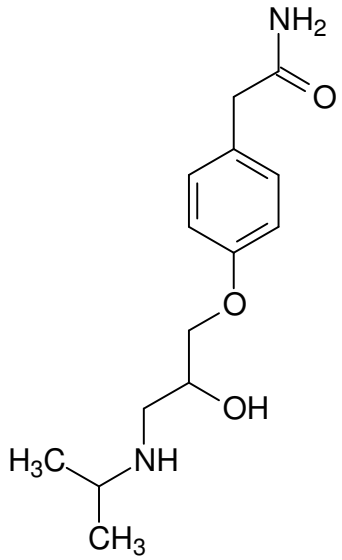

Figure 4.8. The structure of atenolol.

The structure of atenolol is given above. Atenolol is a β-blocking agent which is used in the treatment of hypertension and angina pectoris (Moneghini *et al.,* 1998). It may also be used in acute myocardial infarction. The results of the MAO inhibition studies show that atenolol is not an inhibitor of either MAO-A and MAO-B, even at a maximal tested concentration of 100 µM. The concentration-response curves of the MAO-A and MAO-B catalytic activity in presence of increasing concentrations of atenolol are given below. The graph shows that there is no significant decrease in the catalytic activities of MAO-A and MAO-B with increasing concentrations of atenolol.

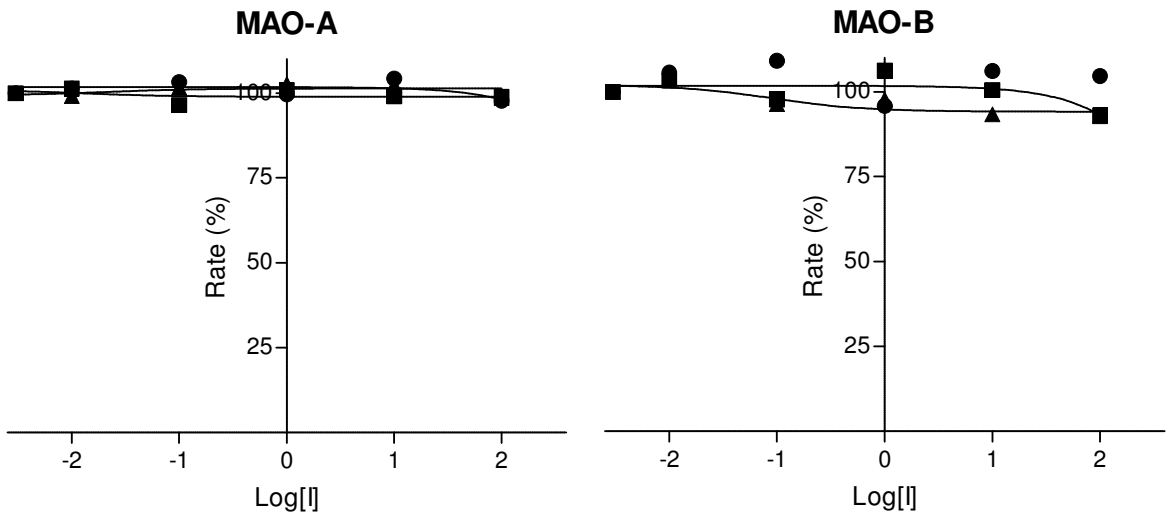

Figure 4.9. The recombinant human MAO-A (left) and MAO-B (right) catalyzed oxidation of kynuramine in the presence of various concentrations of atenolol (expressed in μM). The concentration-response curves were constructed in triplicate from the initial rates of kynuramine oxidation versus the logarithm of the concentration of atenolol. The rates are expressed as the percentage of the catalytic rate recorded in the absence of inhibitor.

4.4.3. Acetaminophen

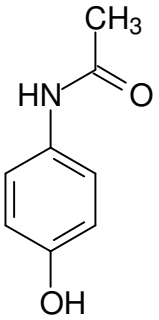

Figure 4.10. The structure of acetaminophen.

The structure of acetaminophen is given above. Acetaminophen or paracetamol is a nonsteroidal anti-inflammatory drug with weak anti-inflammatory activity but has potent antipyretic and analgesic actions (Botting, 2000). It is used in the treatment of mild to moderate painful conditions. The results of the MAO inhibition studies show that acetaminophen is not an inhibitor of either MAO-A and MAO-B, even at a maximal tested concentration of 100 µM. The concentration-response curves of the MAO-A and MAO-B catalytic activity in presence of increasing concentrations of acetaminophen are given below. The graph shows that there is no significant decrease in the catalytic activities of MAO-A and MAO-B with increasing concentrations of acetaminophen.

.

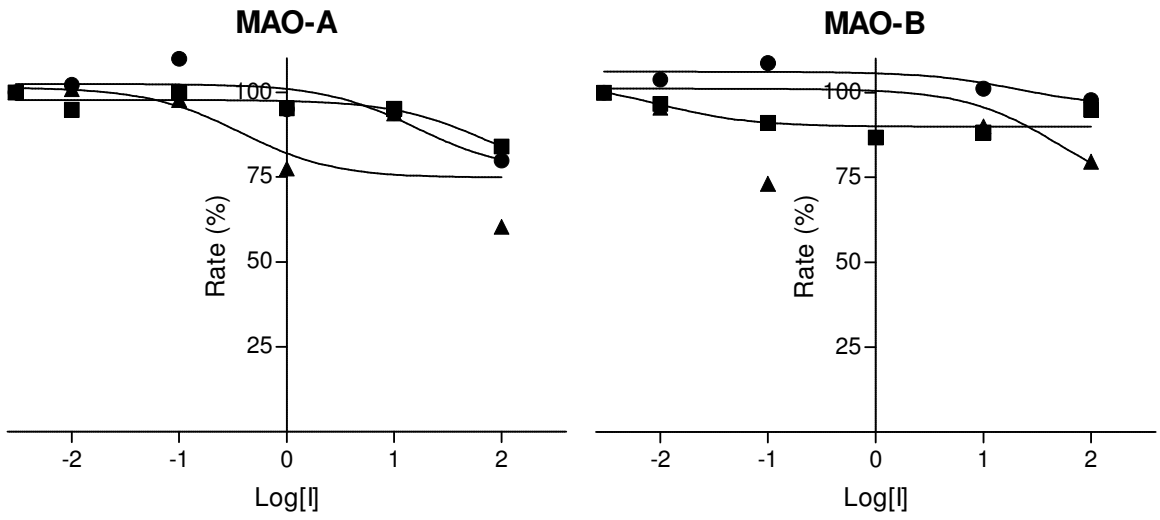

Figure 4.11. The recombinant human MAO-A (left) and MAO-B (right) catalyzed oxidation of kynuramine in the presence of various concentrations of acetaminophen (expressed in µM). The concentration-response curves were constructed in triplicate from the initial rates of kynuramine oxidation versus the logarithm of the concentration of acetaminophen. The rates are expressed as the percentage of the catalytic rate recorded in the absence of inhibitor.

4.4.4. Betaxolol

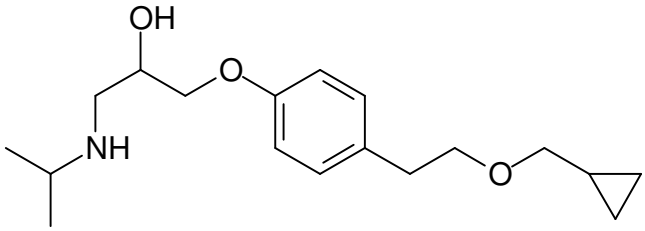

Figure 4.12. The structure of betaxolol.

The structure of betaxolol is given above. Betaxolol is a selective β_1-adrenoreceptor antagonist which is frequently used in the management of glaucoma. Betaxolol decreases intraocular pressure and it also acts as a calcium channel blocker (Cheon *et al*., 2006). Betaxolol is used in the treatment of glaucoma (as mentioned above) and systemic hypertension (Melena *et al*., 1999). The results of the MAO inhibition studies show that betoxalol is not a significant inhibitor of either MAO-A and MAO-B. At a maximal tested concentration of 100 µM a small degree of inhibition of both MAO-A and MAO-B is observed in one replicate determination. The concentration-response curves of the MAO-A and MAO-B catalytic activity in presence of increasing concentrations of betoxalol are given below. The graph shows that the small decrease in the catalytic activities of MAO-A and MAO-B at 100 µM is only 33% and 37%, respectively. This decrease is only observed with one replicate of the triplicate determinations and may be due to experimental error.

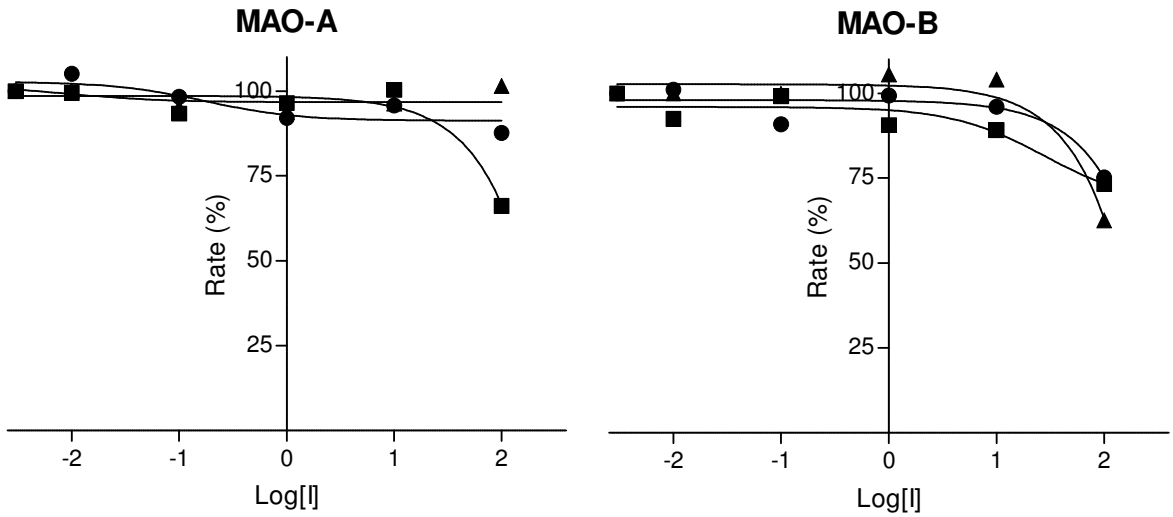

Figure 4.13. The recombinant human MAO-A (left) and MAO-B (right) catalyzed oxidation of kynuramine in the presence of various concentrations of betoxalol (expressed in μM). The concentration-response curves were constructed in triplicate from the initial rates of kynuramine oxidation versus the logarithm of the concentration of betoxalol. The rates are expressed as the percentage of the catalytic rate recorded in the absence of inhibitor.

4.4.5. Esmolol

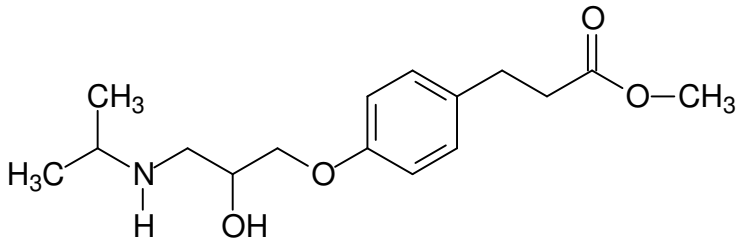

Figure 4.14. The structure of esmolol.

The structure of esmolol is given above. Esmolol is an ultra-short-acting β_1-selective adrenergic antagonist. It is used to control tachycardia/tachyarrhythmia preoperatively in patients with chronic obstructive pulmonary disease and/or asthma, because of its short duration of action and relative lack of effect on airway resistance (Yamakage *et al.*,

2009). The results of the MAO inhibition studies show that esmolol is not an inhibitor of either MAO-A or MAO-B, even at a maximal tested concentration of 100 µM. The concentration-response curves of the MAO-A and MAO-B catalytic activity in presence of increasing concentrations of esmolol are given below. The graph shows that there is no significant decrease in the catalytic activities of MAO-A and MAO-B with increasing concentrations of esmolol.

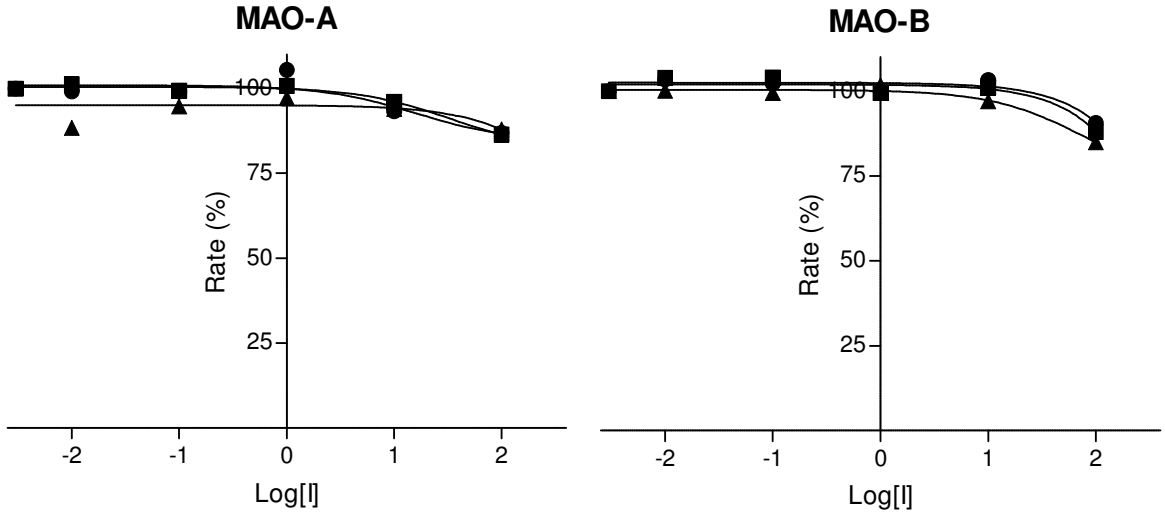

Figure 4.15. The recombinant human MAO-A (left) and MAO-B (right) catalyzed oxidation of kynuramine in the presence of various concentrations of esmolol (expressed in µM). The concentration-response curves were constructed in triplicate from the initial rates of kynuramine oxidation versus the logarithm of the concentration of esmolol. The rates are expressed as the percentage of the catalytic rate recorded in the absence of inhibitor.

4.4.6. Ethambutol

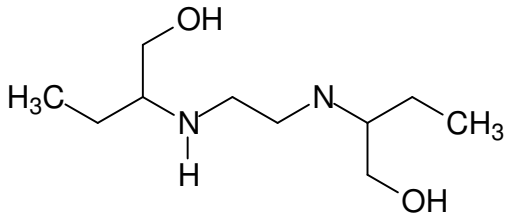

Figure 4.16. The structure of ethambutol.

The structure of ethambutol is given above. Ethambutol inhibits arabinosyl transferases involved in cell-wall biosynthesis. It is active against M. tuberculosis, M. kansasii as well as M. avium complex (Brennan & Young, 2008). The results of the MAO inhibition studies show that ethambutol is not a significant inhibitor of either MAO-A and MAO-B. At a maximal tested concentration of 100 µM a small degree of inhibition of MAO-B is observed in one replicate determination. The concentration-response curves of the MAO-A and MAO-B catalytic activity in presence of increasing concentrations of ethambutol are given below. The graph shows that the small decrease in the catalytic activities of MAO-B at 100 µM is only 30%. This decrease is only observed with one replicate of the determinations.

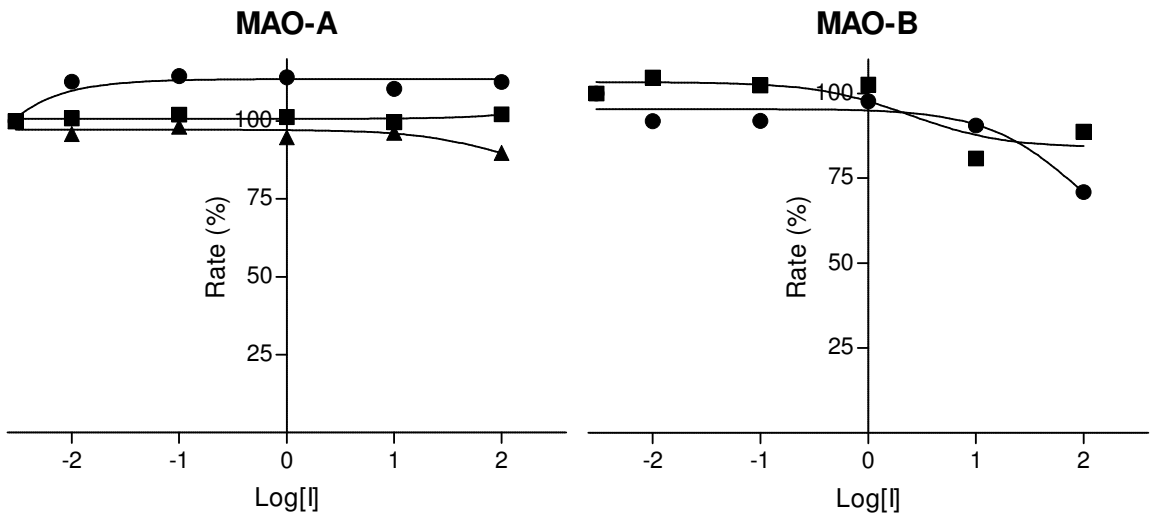

Figure 4.17. The recombinant human MAO-A (left) and MAO-B (right) catalyzed oxidation of kynuramine in the presence of various concentrations of etambutol (expressed in µM). The concentration-response curves were constructed in triplicate (for MAO-A) and duplicate (for MAO-B) from the initial rates of kynuramine oxidation versus the logarithm of the concentration of etambutol. The rates are expressed as the percentage of the catalytic rate recorded in the absence of inhibitor.

4.4.7. Flurbiprofen

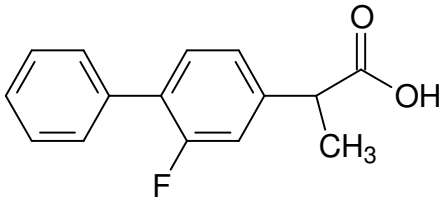

Figure 4.18. The structure of flurbiprofen.

The structure of flurbiprofen is given above. Flurbiprofen is a nonsteroidal anti-inflammatory drug. Flurbiprofen is used in the treatment of pain associated with rheumatoid arthritis and osteoarthritis as well as soft tissue injuries (Liu *et al*., 2009). It may also be used in the treatment of gout and sunburn (Fang *et al*., 2003).The results of the MAO inhibition studies show that flurbiprofen is not an inhibitor of either MAO-A

and MAO-B, even at a maximal tested concentration of 100 µM. The concentration-response curves of the MAO-A and MAO-B catalytic activity in presence of increasing concentrations of flurbiprofen are given below. The graph shows that there is no significant decrease in the catalytic activities of MAO-A and MAO-B with increasing concentrations of flurbiprofen.

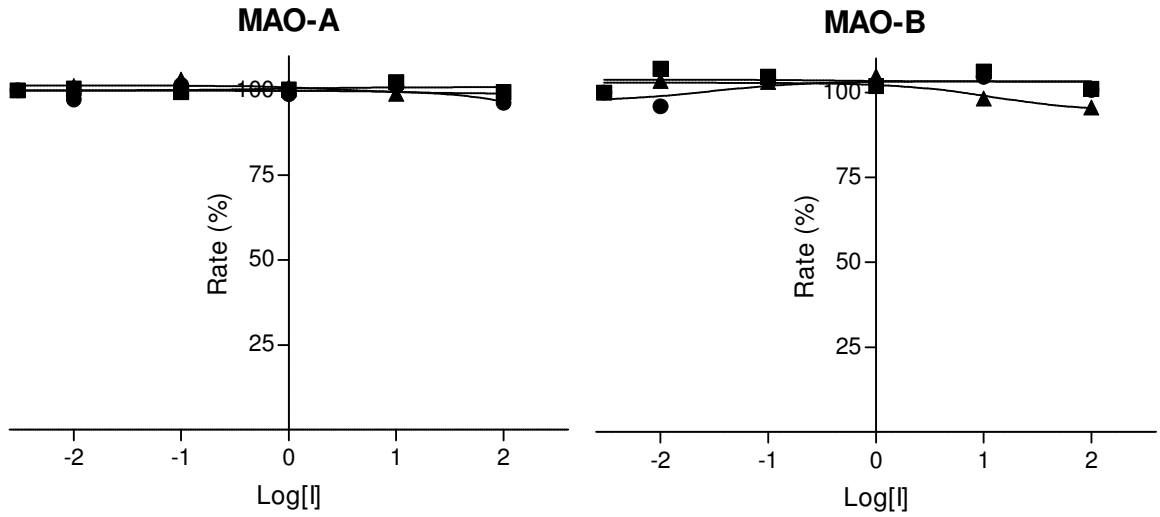

Figure 4.19. The recombinant human MAO-A (left) and MAO-B (right) catalyzed oxidation of kynuramine in the presence of various concentrations of flurbiprofen (expressed in µM). The concentration-response curves were constructed in triplicate from the initial rates of kynuramine oxidation versus the logarithm of the concentration of flurbiprofen. The rates are expressed as the percentage of the catalytic rate recorded in the absence of inhibitor.

4.4.8. Midodrine

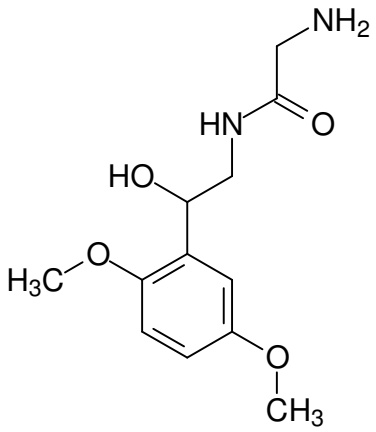

Figure 4.20. The structure of midodrine.

The structure of midodrine is given above. Midodrine is an α-agonist prodrug of desglymidodrine. Midodrine may be beneficial in patients with neurocardiogenic syncope (Lamarre-Cliche *et al*., 2008). The results of the MAO inhibition studies show that midodrine is not an inhibitor of either MAO-A and MAO-B, even at a maximal tested concentration of 100 µM. The concentration-response curves of the MAO-A and MAO-B catalytic activity in presence of increasing concentrations of midodrine are given below. The graph shows that there is no significant decrease in the catalytic activities of MAO-A and MAO-B with increasing concentrations of midodrine.

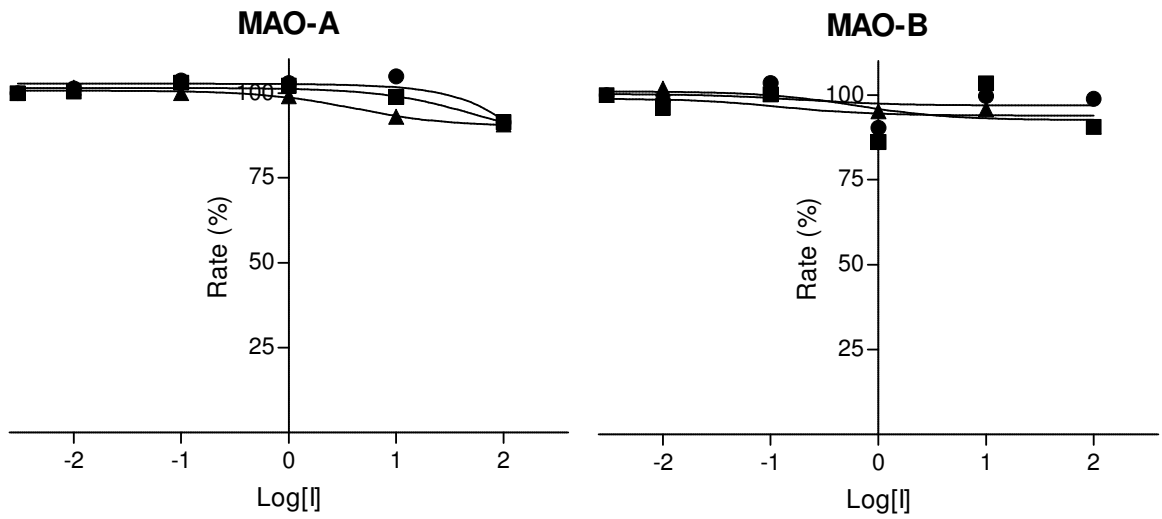

Figure 4.21. The recombinant human MAO-A (left) and MAO-B (right) catalyzed oxidation of kynuramine in the presence of various concentrations of midodrine (expressed in µM). The concentration-response curves were constructed in triplicate from the initial rates of kynuramine oxidation versus the logarithm of the concentration of midodrine. The rates are expressed as the percentage of the catalytic rate recorded in the absence of inhibitor.

4.4.9. Milrinone

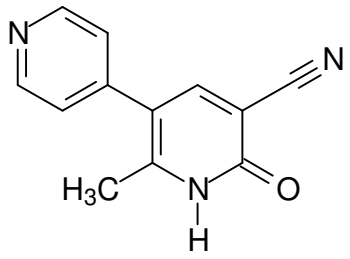

Figure 4.22. The structure of milrinone.

The structure of milrinone is given above. Milrinone is a phosphodiesterase-3 inhibitor. Milrinone is used during cardiac surgery when the cardiac output is low immediately after anesthetic induction. Milrinone contributes to the adjustment of oxygen supply to the tissue, preventing organ dysfunction (Carmona *et al*., 2010). The results of the MAO

inhibition studies show that milrinone is not an inhibitor of either MAO-A and MAO-B, even at a maximal tested concentration of 100 µM. The concentration-response curves of the MAO-A and MAO-B catalytic activity in presence of increasing concentrations of milrinone are given below. The graph shows that there is no significant decrease in the catalytic activities of MAO-A and MAO-B with increasing concentrations of milrinone.

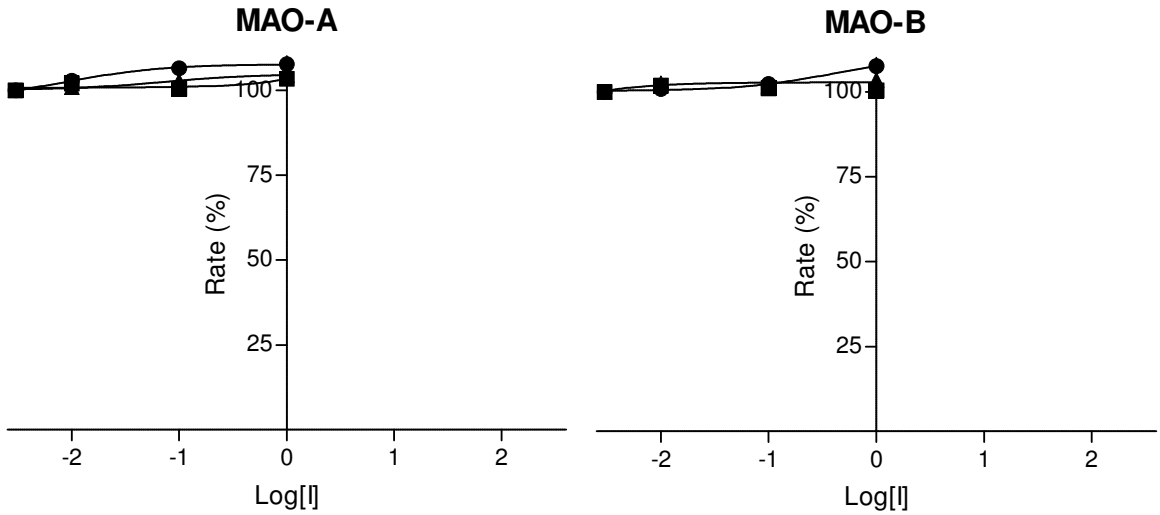

Figure 4.23. The recombinant human MAO-A (left) and MAO-B (right) catalyzed oxidation of kynuramine in the presence of various concentrations of milrinone (expressed in µM). The concentration-response curves were constructed in triplicate (for MAO-A) and duplicate (for MAO-B) from the initial rates of kynuramine oxidation versus the logarithm of the concentration of milrinone. The rates are expressed as the percentage of the catalytic rate recorded in the absence of inhibitor. This compound was evaluated to a maximal concentration of only 1 µM since it fluoresced at higher concentrations, and thus affected the measurement of the fluorescence of 4-hydroxyquinoline.

4.4.10. Minaprine

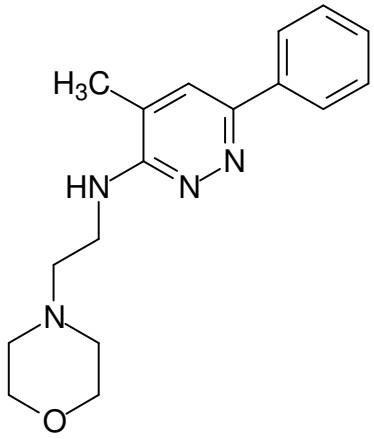

Figure 4.24. The structure of minaprine.

The structure of minaprine is given above. Minaprine is an atypical antidepressant and inhibits the reuptake of serotonin. Minaprine is commonly used in the treatment of depression in the elderly because it is devoid of cardiovascular side-effects (Gareri *et al*., 1998). The results of the MAO inhibition studies show that minaprine is not a significant inhibitor of either MAO-A and MAO-B. At a maximal tested concentration of 100 µM a small degree of in inhibition of MAO-B is observed in one replicate determination. The concentration-response curves of the MAO-A and MAO-B catalytic activity in presence of increasing concentrations of minaprine are given below. The graph shows that the small decrease in the catalytic activities of MAO-B at 100 µM is only 37%. This decrease is only observed with one replicate of the triplicate determinations.

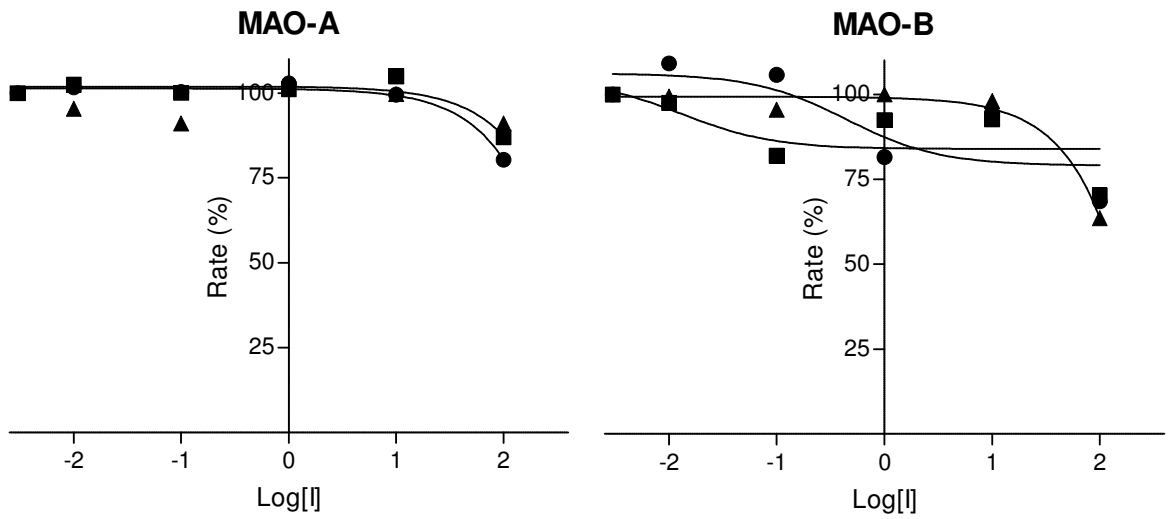

Figure 4.25. The recombinant human MAO-A (left) and MAO-B (right) catalyzed oxidation of kynuramine in the presence of various concentrations of minaprine (expressed in µM). The concentration-response curves were constructed in triplicate from the initial rates of kynuramine oxidation versus the logarithm of the concentration of minaprine. The rates are expressed as the percentage of the catalytic rate recorded in the absence of inhibitor.

4.4.11. Naproxen

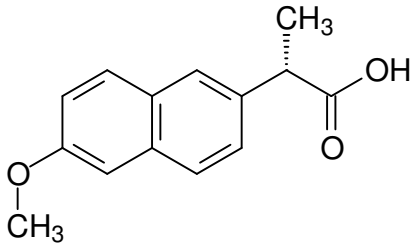

Figure 4.26. The structure of naproxen.

The structure of naproxen is given above. Naproxen is a nonsteroidal anti-inflammatory drug. It has inhibitory effects on COX-1 and COX-2 and has a smaller cardiovascular risk in higher doses than other nonsteroidal anti-inflammatory drugs (Capone *et al*., 2007). It may be used in the treatment of inflammatory disorders such as gout. The

results of the MAO inhibition studies show that naproxen is not an inhibitor of either MAO-A and MAO-B, even at a maximal tested concentration of 100 µM. The concentration-response curves of the MAO-A and MAO-B catalytic activity in presence of increasing concentrations of naproxen are given below. The graph shows that there is no significant decrease in the catalytic activities of MAO-A and MAO-B with increasing concentrations of naproxen.

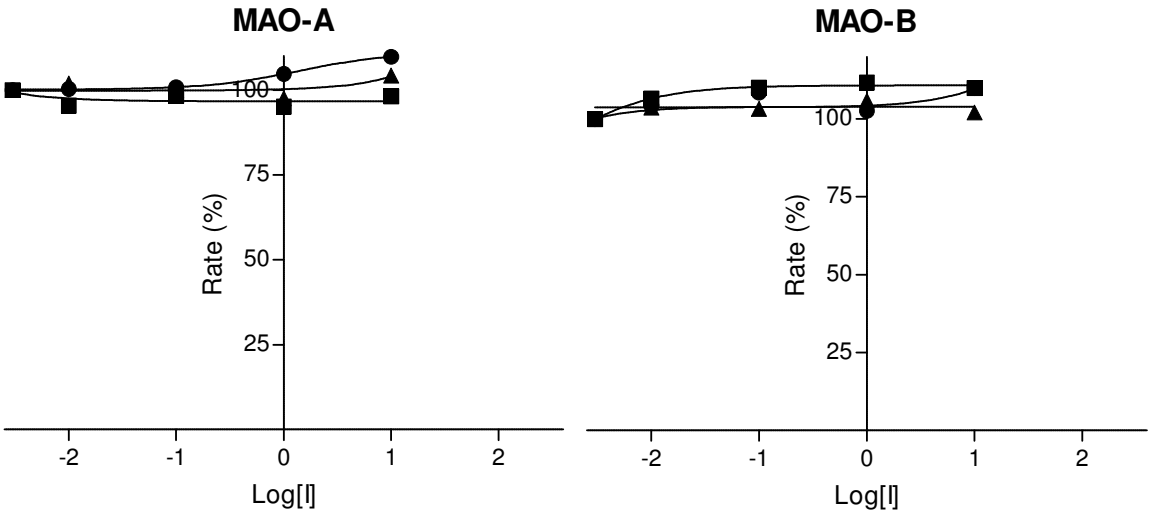

Figure 4.27. The recombinant human MAO-A (left) and MAO-B (right) catalyzed oxidation of kynuramine in the presence of various concentrations of naproxen (expressed in µM). The concentration-response curves were constructed in triplicate from the initial rates of kynuramine oxidation versus the logarithm of the concentration of naproxen. The rates are expressed as the percentage of the catalytic rate recorded in the absence of inhibitor. This compound was evaluated to a maximal concentration of only 10 µM since it fluoresced at higher concentrations, and thus affected the measurement of the fluorescence of 4-hydroxyquinoline.

4.4.12. Propranolol

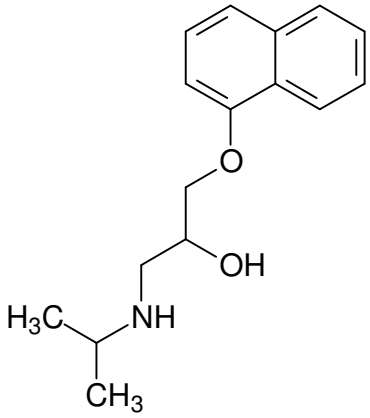

Figure 4.28. The structure of propranolol.

The structure of propranolol is given above. Propranolol is a β-adrenergic blocking agent which may be used in the treatment of various diseases including hypertension, angina and it has antiarrhythmic activity (Nies & Shand, 1975). It may also be effective in relieving migraine and states of anxiety. The results of the MAO inhibition studies show that propranolol is not an inhibitor of either MAO-A and MAO-B, even at a maximal tested concentration of 100 μM. The concentration-response curves of the MAO-A and MAO-B catalytic activity in presence of increasing concentrations of propranolol are given below. The graph shows that there is no significant decrease in the catalytic activities of MAO-A and MAO-B with increasing concentrations of propranolol.

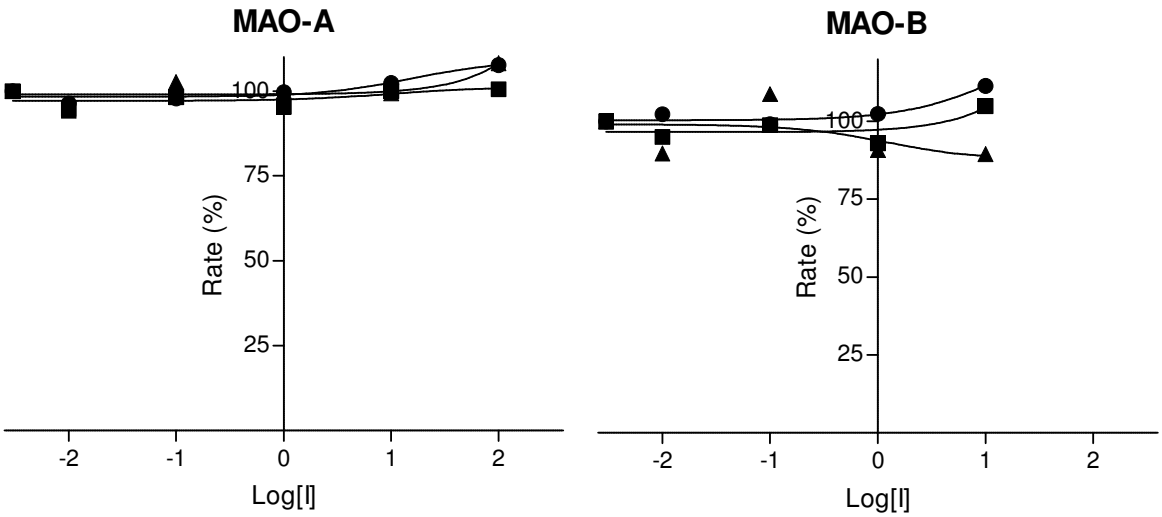

Figure 4.29. The recombinant human MAO-A (left) and MAO-B (right) catalyzed oxidation of kynuramine in the presence of various concentrations of propranolol (expressed in μM). The concentration-response curves were constructed in triplicate from the initial rates of kynuramine oxidation versus the logarithm of the concentration of propranolol. The rates are expressed as the percentage of the catalytic rate recorded in the absence of inhibitor. For the measurement with MAO-B, this compound was evaluated to a maximal concentration of only 10 μM since it fluoresced at higher concentrations, and thus affected the measurement of the fluorescence of 4-hydroxyquinoline.

4.4.13. Ritodrine

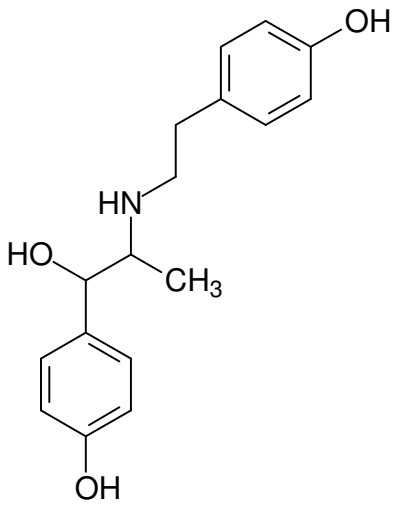

Figure 4.30. The structure of ritodrine.

The structure of ritodrine is given above. Ritodrine is a β-sympathomimetic agent with predominant effects on β_2-receptors of the uterus. It is the first drug to be approved in the United States for the specific use in preterm labor (Barden *et al.*, 1980). Ritodrine may inhibit preterm labor by up to seven days. The results of the MAO inhibition studies show that ritodrine is not an inhibitor of either MAO-A and MAO-B, even at a maximal tested concentration of 100 μM. The concentration-response curves of the MAO-A and MAO-B catalytic activity in presence of increasing concentrations of ritodrine are given below. The graph shows that there is no significant decrease in the catalytic activities of MAO-A and MAO-B with increasing concentrations of ritodrine.

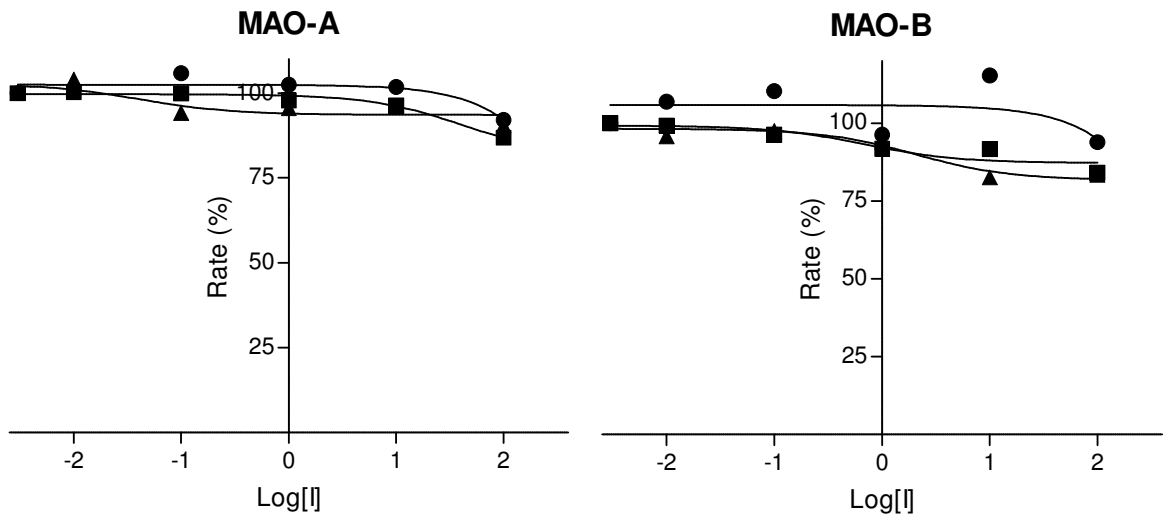

Figure 4.31. The recombinant human MAO-A (left) and MAO-B (right) catalyzed oxidation of kynuramine in the presence of various concentrations of ritodrine (expressed in μM). The concentration-response curves were constructed in triplicate from the initial rates of kynuramine oxidation versus the logarithm of the concentration of ritodrine. The rates are expressed as the percentage of the catalytic rate recorded in the absence of inhibitor.

4.4.14. Sulfanilamide

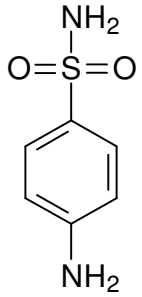

Figure 4.32. The structure of sulfanilamide.

The structure of sulfanilamide is given above. Sulfanilamide is part of a group of pharmaceuticals known as sulfa drugs which is widely used as effective chemotherapeutic agents for the prevention and treatment of bacterial infections and

may be used in the treatment of various diseases including meningitis, tonsillitis, gonorrhea, pneumonia and sinus infections (Ildiz & Akyuz, 2012). It may also be used in the treatment of glaucoma (Turkman *et al*., 2011). The results of the MAO inhibition studies show that sulfanilamide is not an inhibitor of either MAO-A and MAO-B, even at a maximal tested concentration of 100 µM. The concentration-response curves of the MAO-A and MAO-B catalytic activity in presence of increasing concentrations of sulfanilamide are given below. The graph shows that there is no significant decrease in the catalytic activities of MAO-A and MAO-B with increasing concentrations of sulfanilamide.

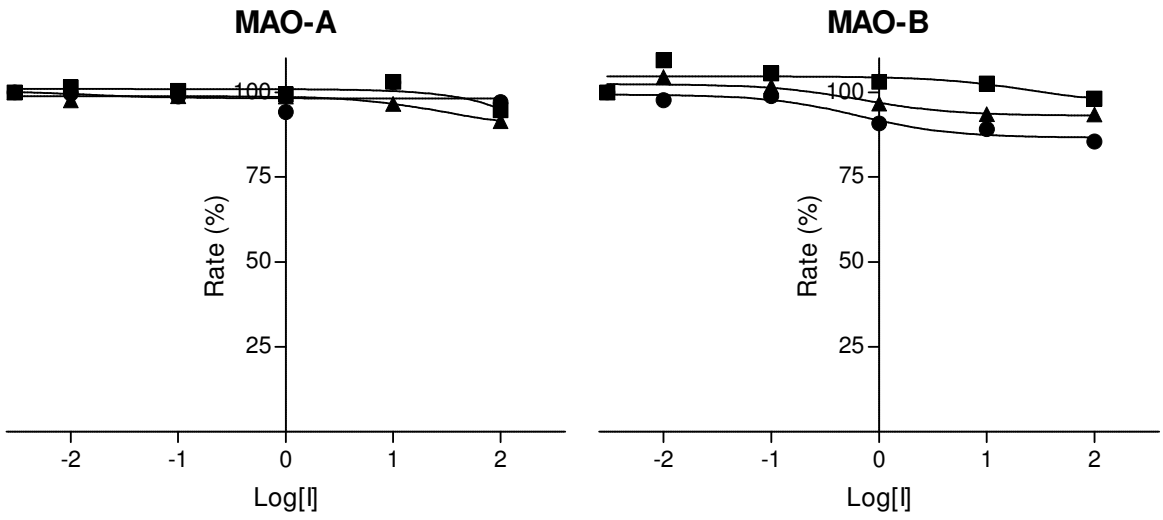

Figure 4.33. The recombinant human MAO-A (left) and MAO-B (right) catalyzed oxidation of kynuramine in the presence of various concentrations of sulfanilamide (expressed in µM). The concentration-response curves were constructed in triplicate from the initial rates of kynuramine oxidation versus the logarithm of the concentration of sulfanilamide. The rates are expressed as the percentage of the catalytic rate recorded in the absence of inhibitor.

4.4.15. Sulfisoxazole

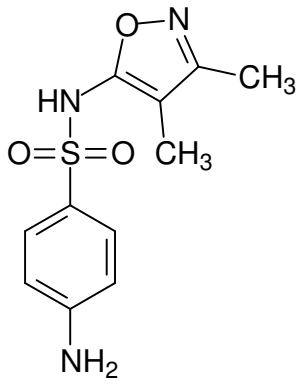

Figure 4.34. The structure of sulfisoxazole.

The structure of sulfisoxazole is given above. Sulfisoxazole is a short acting sulfonamide antibiotic. It may be used in the treatment of acute uncomplicated urinary tract infections, otitis media, chancroid, cystitis in women who are not pregnant and it is the preferred sulfonamide for susceptible systemic infections (Connor, 1998). The results of the MAO inhibition studies show that sulfisoxazole is not an inhibitor of either MAO-A and MAO-B, even at a maximal tested concentration of 100 μM. The concentration-response curves of the MAO-A and MAO-B catalytic activity in presence of increasing concentrations of sulfisoxazole are given below. The graph shows that there is no significant decrease in the catalytic activities of MAO-A and MAO-B with increasing concentrations of sulfisoxazole.

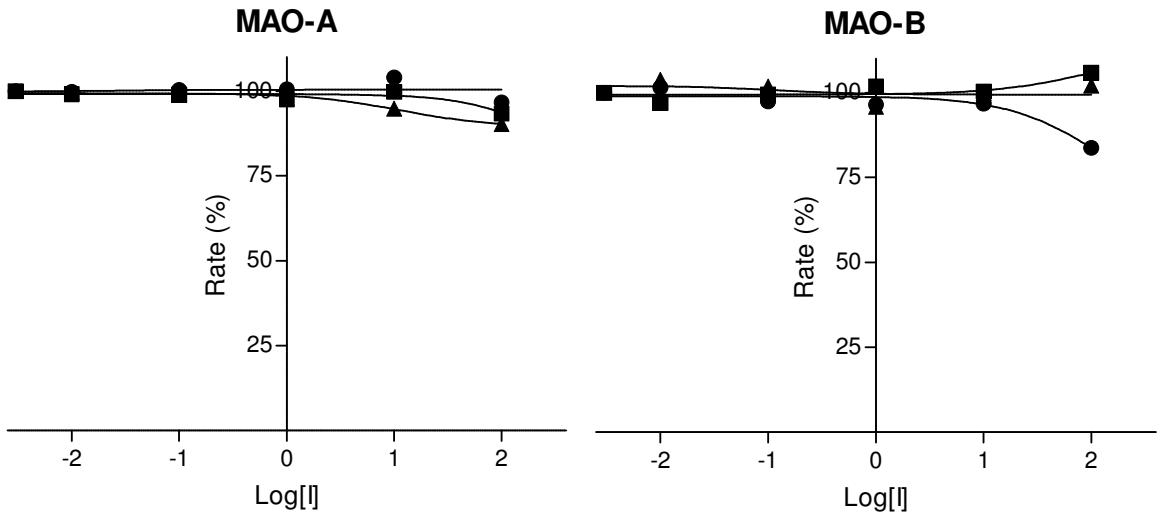

Figure 4.35. The recombinant human MAO-A (left) and MAO-B (right) catalyzed oxidation of kynuramine in the presence of various concentrations of sulfisoxazole (expressed in μM). The concentration-response curves were constructed in triplicate from the initial rates of kynuramine oxidation versus the logarithm of the concentration of sulfisoxazole. The rates are expressed as the percentage of the catalytic rate recorded in the absence of inhibitor.

4.4.16. Tramadol

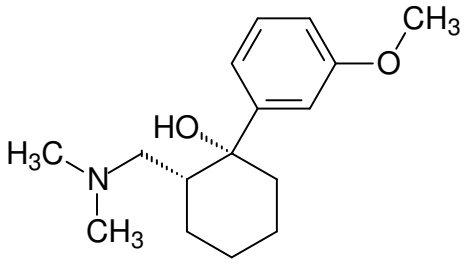

Figure 4.36. The structure of tramadol.

The structure of tramadol is given above. Tramadol is an opioid agonist and has analgesic activity. Tramadol also inhibits the spinal re-uptake of noradrenaline and serotonin. Tramadol is used in the treatment of acute pain including pain caused by trauma, acute myocardial infarction, dental pain and smooth muscle spasms (Budd,

1999). The results of the MAO inhibition studies show that tramadol is not a significant inhibitor of either MAO-A and MAO-B. At a maximal tested concentration of 100 µM a small degree of inhibition of MAO-B is observed in one replicate determination. The concentration-response curves of the MAO-A and MAO-B catalytic activity in presence of increasing concentrations of tramadol are given below. The graph shows that the small decrease in the catalytic activities of MAO-B at 100 µM is only 25%. This decrease is only observed with one replicate of the triplicate determinations.

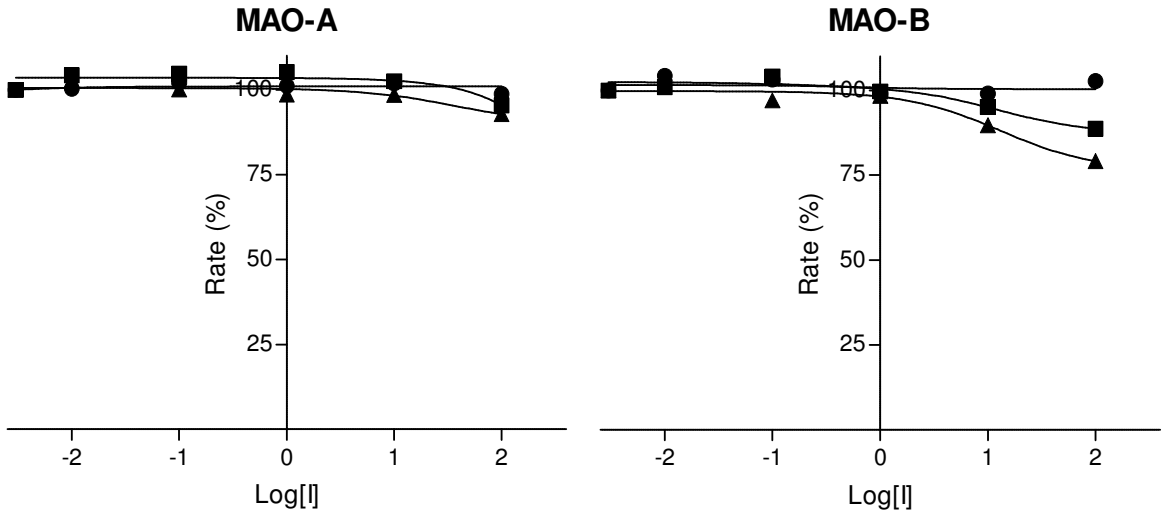

Figure 4.37. The recombinant human MAO-A (left) and MAO-B (right) catalyzed oxidation of kynuramine in the presence of various concentrations of tramadol (expressed in µM). The concentration-response curves were constructed in triplicate (for MAO-A) and duplicate (for MAO-B) from the initial rates of kynuramine oxidation versus the logarithm of the concentration of tramadol. The rates are expressed as the percentage of the catalytic rate recorded in the absence of inhibitor.

4.5. Results of the MAO inhibition studies with those drugs which proved to be MAO inhibitors *in vitro*.

4.5.1. Anagrelide

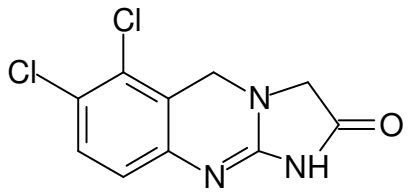

Figure 4.38. The structure of anagrelide.

The structure of anagrelide is given above. Anagrelide is an anti-thrombotic agent and is used in the treatment of essential thrombocythemia (Petrides *et al*., 2009). The results of the MAO inhibition studies show that anagrelide is an inhibitor of both MAO-A and MAO-B. The concentration-response curves of the MAO-A and MAO-B catalytic activity in presence of increasing concentrations of anagrelide are given below. The graph shows that there is a significant decrease in the catalytic activities of MAO-A and MAO-B with increasing concentrations of anagrelide. Maximal suppression of MAO-A and MAO-B activities were, however, not achieved with the maximal concentration tested 100 µM. The IC_{50} values recorded for the inhibition of MAO-A and MAO-B are estimated at 48.7 ± 4.20 µM and 115 ± 18.7 µM, respectively.

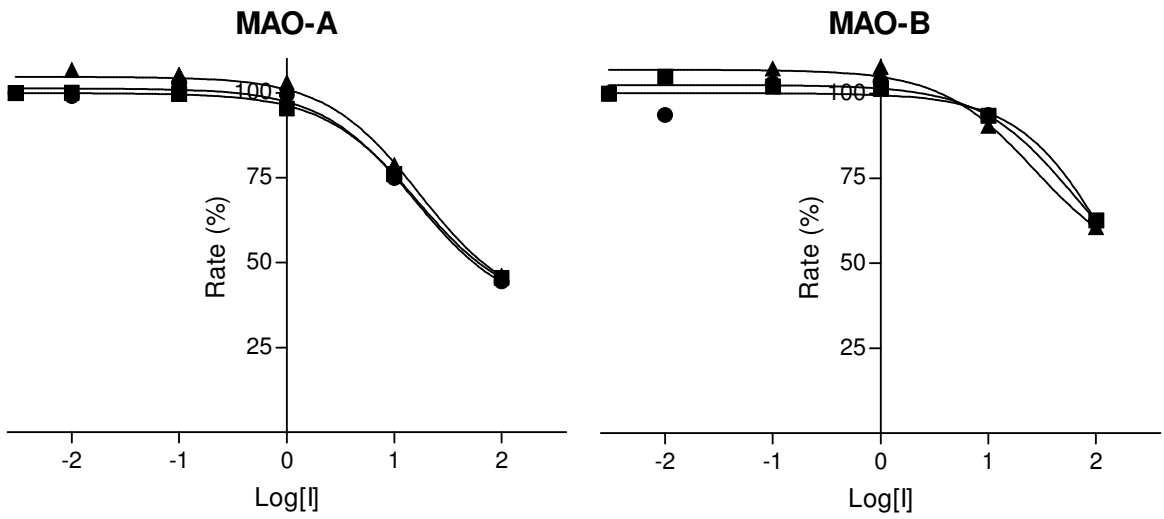

Figure 4.39. The recombinant human MAO-A (left) and MAO-B (right) catalyzed oxidation of kynuramine in the presence of various concentrations of anagrelide (expressed in μM). The concentration-response curves were constructed from the initial rates of kynuramine oxidation versus the logarithm of the concentration of anagrelide. The rates are expressed as the percentage of the catalytic rate recorded in the absence of inhibitor.

4.5.2. Apomorphine

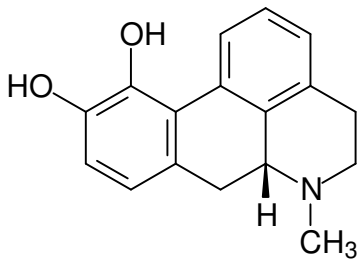

Figure 4.40. The structure of apomorphine.

The structure of apomorphine is given above. Apomorphine is a known inhibitor of MAO. Apomorphine is a D_1 and D_2 dopaminergic agonist. Apomorphine is used to increase the duration of "*on*" periods in Parkinson's disease and to ameliorate the "*off*" phases of Parkinson's disease (Muguet *et al.*, 1995). The results of the MAO inhibition

studies show that apomorphine is an inhibitor of both MAO-A and MAO-B. The concentration-response curves of the MAO-A and MAO-B catalytic activity in presence of increasing concentrations of apomorphine are given below. The graph shows that there is a significant decrease in the catalytic activities of MAO-A and MAO-B with increasing concentrations of apomorphine. Maximal suppression of MAO-A and MAO-B activities were, however, not achieved with the maximal concentration tested 100 µM. The IC_{50} values recorded for the inhibition of MAO-A and MAO-B are estimated at 26.4 ± 5.5 µM and 39.1 ± 5.9 µM, respectively.

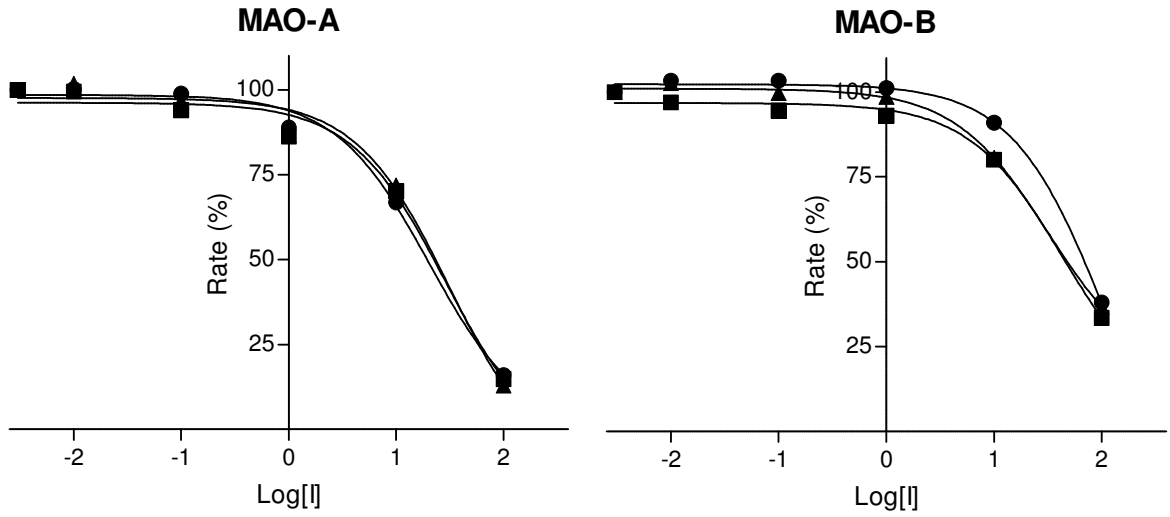

Figure 4.41. The recombinant human MAO-A (left) and MAO-B (right) catalyzed oxidation of kynuramine in the presence of various concentrations of apomorphine (expressed in µM). The concentration-response curves were constructed from the initial rates of kynuramine oxidation versus the logarithm of the concentration of apomorphine. The rates are expressed as the percentage of the catalytic rate recorded in the absence of inhibitor.

4.5.3. Caffeine

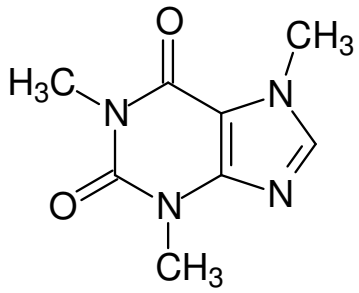

Figure 4.42. The structure of caffeine.

The structure of caffeine is given above. Studies have shown that caffeine may be used to protect against Alzheimer's disease (Dragicevic *et al*., 2012). Caffeine may also reduce the risk of developing Parkinson's disease because of the antagonistic effect of caffeine at the A_{2A} adenosine receptors in the striatum (Lorist *et al*., 2003). The results of the MAO inhibition studies show that caffeine is an inhibitor of both MAO-A and MAO-B with IC_{50} values of 0.761 ± 0.040 mM and 5.08 ± 1.09 mM, respectively. The concentration-response curves of the MAO-A and MAO-B catalytic activities in presence of increasing concentrations of caffeine are given below. The graph shows that there is a decrease in the catalytic activities of both MAO-A and MAO-B with increasing concentrations of caffeine. Although caffeine is a relatively weak MAO inhibitor, this molecule is of high dietary importance and the interactions of caffeine with these enzymes were thus further investigated. The interactions of caffeine with the MAOs will be further analysed in Chapter 6 where these results will be presented as a concept article.

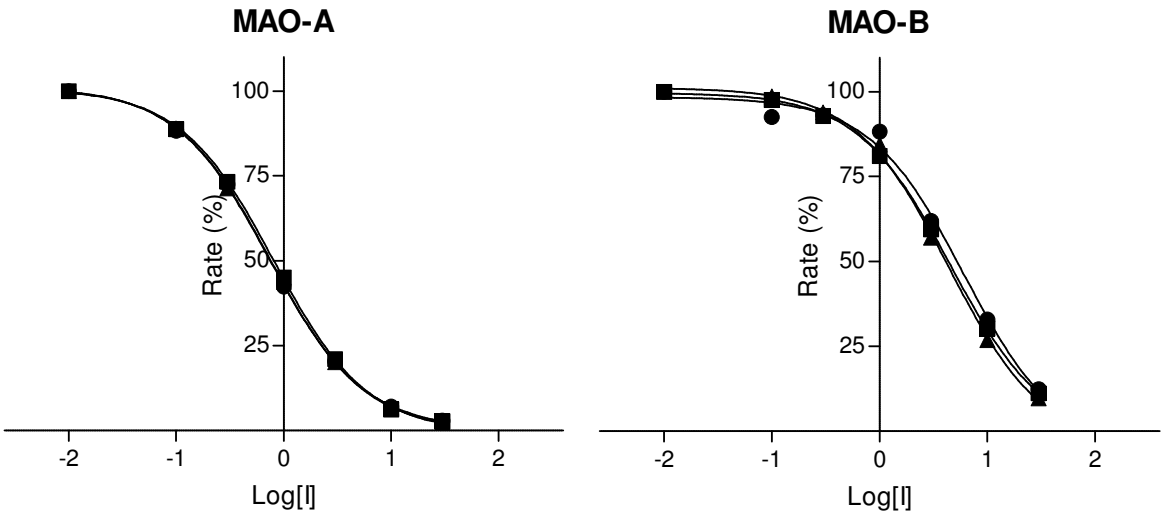

Figure 4.43. The recombinant human MAO-A (left) and MAO-B (right) catalyzed oxidation of kynuramine in the presence of various concentrations of caffeine (expressed in mM). The concentration-response curves were constructed from the initial rates of kynuramine oxidation versus the logarithm of the concentration of caffeine. The rates are expressed as the percentage of the catalytic rate recorded in the absence of inhibitor.

The reversibility of MAO-A and MAO-B inhibition by caffeine was investigated by measuring the recoveries of enzyme activities after dialysis of enzyme-inhibitor mixtures (Harfenist *et al.*, 1996). The MAO enzymes and caffeine, at a concentration of 4 × IC_{50}, were preincubated for a period of 15 min and subsequently dialyzed for 24 h. The results, given in Fig. 4.44, show that MAO-A and MAO-B inhibition by caffeine is almost completely reversed after 24 h of dialysis with the MAO-A and MAO-B activities recovering to levels of 97% and 96% of the control values (recorded in the absence of inhibitor), respectively. In contrast, the MAO-A and MAO-B activities in undialyzed mixtures of the enzymes with caffeine are 37% and 39%, respectively, of the control values. This behaviour is consistent with a reversible interaction between the MAO enzymes and caffeine. For comparison, after similar preincubation and dialysis of MAO-A and MAO-B with the irreversible inhibitors, pargyline and (R)-deprenyl, respectively, the enzyme activities are not recovered. After dialysis of MAO-A–pargyline and MAO-B–

(R)-deprenyl mixtures, the residual enzyme activities are recovered to levels of only 4.4% and 2.8%, respectively, of the control values.

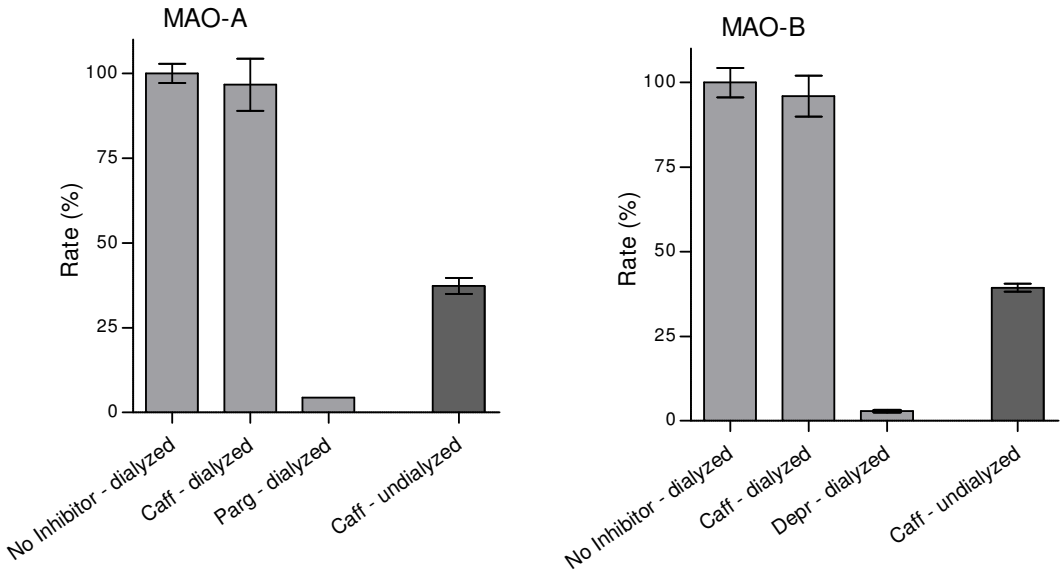

Figure 4.44. Reversibility of inhibition of human MAO-A (left) and MAO-B (right) by caffeine. MAO-A and MAO-B were preincubated for a period of 15 min with caffeine, at a concentration of 4 × IC_{50}. The mixtures were dialyzed for 24 h and the residual MAO activities were measured (Caff–dialyzed). For comparison, the MAOs were similarly preincubated in the absence (No inhibitor–dialyzed) and presence of the irreversible inhibitors, pargyline (Parg–dialyzed) and (R)-deprenyl (Depr–dialyzed), respectively, and dialyzed. The residual MAO activities of undialyzed mixtures of MAO-A and MAO-B with caffeine (Caff–undialyzed) are also shown.

The modes of MAO-A and MAO-B inhibition by caffeine were investigated by constructing a set of Lineweaver–Burk plots for the inhibition of MAO-A and MAO-B. The catalytic rates were measured in the presence of five different concentrations of caffeine, and in the absence of caffeine. These measurements were carried out using eight different concentrations of the substrate, kynuramine (15–250 μM). Figure 4.45 illustrates the set of Lineweaver–Burk plots that were obtained from these studies. The results show that the Lineweaver–Burk plots are linear and intersect at a single point on

the y-axis. This suggests that caffeine most likely interacts competitively with both MAO isozymes.

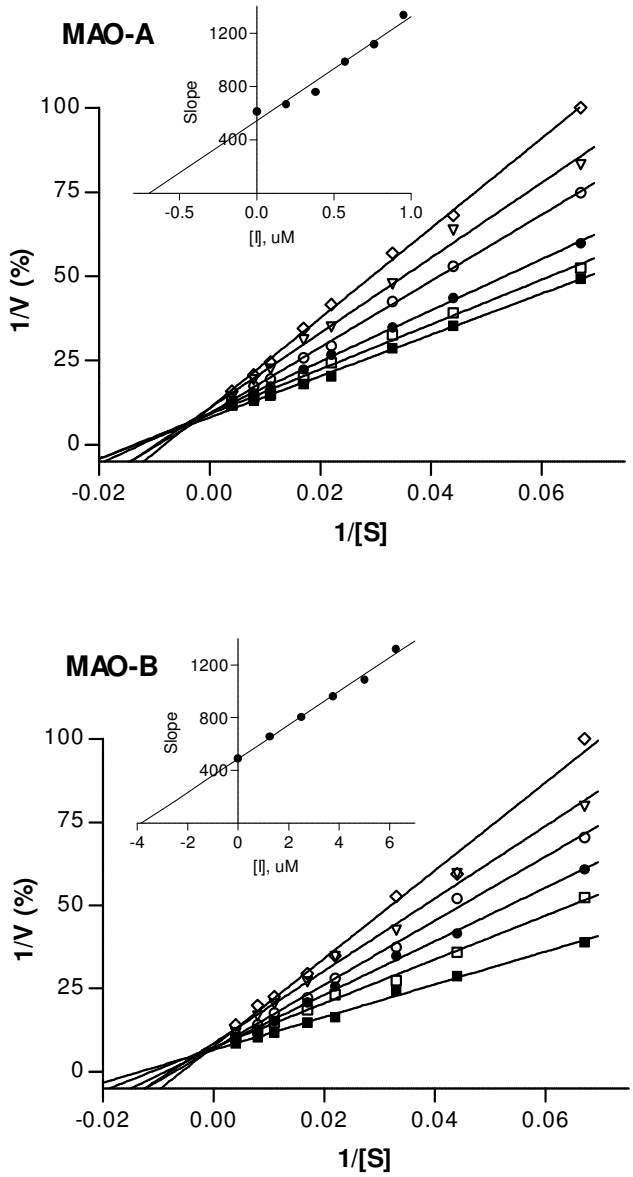

Figure 4.45. Lineweaver-Burk plots of the oxidation of kynuramine by recombinant human MAO-A (top) and MAO-B (bottom). The plots were constructed in the absence (filled squares) and presence of various concentrations of caffeine. The concentrations of caffeine employed were ¼ × IC_{50} (open squares), ½ × IC_{50} (filled circles), ¾ × IC_{50} (open circles), 1 × IC_{50} (triangles) and 1¼ × IC_{50} (diamonds), respectively.

To provide additional insight, the binding modes of caffeine within the active site cavities of MAO-A and MAO-B were examined. The molecular docking simulations were carried out according to the protocol given in Chapter 2. The results are given in figure 4.46 and tables 4.2 and 4.3. As shown in the three-dimensional representations, in the MAO-A active site, caffeine undergoes π-π interactions with Tyr407 and hydrogen bonding with the phenolic hydrogen of Tyr444. The π-π interaction contribute significantly to the total binding energy of the ligand (–3.62 kcal/mol). Significant interactions (hydrophobic) also occur between caffeine and Ile180, Gln215, Phe352 and the FAD cofactor. The interaction energies show that these amino acid residues contribute significantly to the total binding energy of the ligand (–3.14, –5.57, –2.54 and –2.65 kcal/mol, respectively). Based on the more negative energies, the interactions with Tyr407 and Gln215 are especially important. Interestingly, caffeine form a non-productive interaction with Asn181 (+15.8 kcal/mol) which may explain the relatively low inhibition potency of caffeine towards MAO-A (IC_{50} = 0.761 mM).

In the MAO-B active site, caffeine undergoes hydrogen bonding with Tyr326. This interaction, however, does not contribute to the total binding energy of the ligand (+10.8 kcal/mol) and represents a non-productive interaction. This interaction may explain the relatively low inhibition potency of caffeine towards MAO-B (IC_{50} = 5.08 mM). Significant interactions (hydrophobic) occur between caffeine and Phe168 (–2.32 kcal/mol), Leu171 (–2.84 kcal/mol), and Ile199 (–7.17 kcal/mol). Based on the more negative energies, the interaction with Ile199 is especially important.

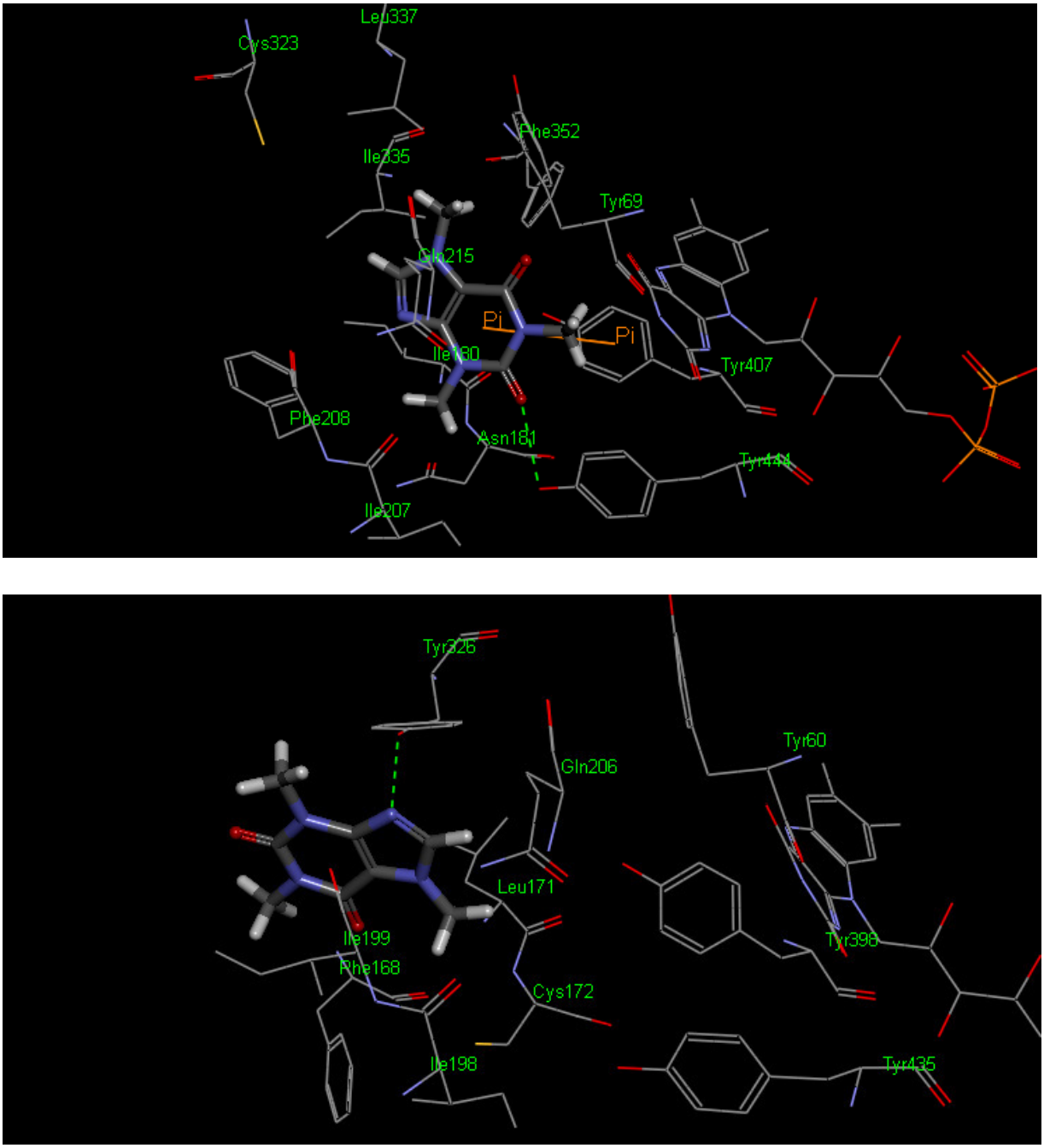

Figure 4.46. The docked orientations of caffeine within the MAO-A (top) and MAO-B (bottom) active sites.

Table 4.1. The principal interaction energies of caffeine with the active site residues of MAO-A.

Name	Forcefield	Total Interaction Energy (kcal/mol)	Total VDW Interaction Energy (kcal/mol)	Total Electrostatic Interaction Energy (kcal/mol)
2Z5X	2Z5X-CHARMm	-14.22218	-12.93440	-1.28777

Interaction Energies				
Conformation	Residue	Interaction Energy (kcal/mol)	VDW Interaction Energy (kcal/mol)	Electrostatic Interaction Energy (kcal/mol)
1	A_TYR69	-1.728820	-1.635140	-0.093684
1	A_VAL70	-0.006441	-0.043195	0.036754
1	A_GLN74	-0.000543	-0.040245	0.039702
1	A_VAL91	-0.134916	-0.050772	-0.084144
1	A_VAL93	-0.007450	-0.005895	-0.001555
1	A_LEU97	0.016760	-0.014202	0.030961
1	A_PHE108	-0.040450	-0.001704	-0.038747
1	A_ALA111	-0.044412	-0.014297	-0.030115
1	A_PHE112	0.020206	-0.019230	0.039436
1	A_ILE180	-3.144850	-2.968540	-0.176310
1	A_ASN181	15.775900	16.175501	-0.399635
1	A_THR183	0.145784	-0.115900	0.261684
1	A_TYR197	-0.273376	-0.180519	-0.092857
1	A_ILE207	-1.829900	-1.684310	-0.145589
1	A_PHE208	-1.470250	-1.608520	0.138265
1	A_SER209	-0.201067	-0.184380	-0.016687
1	A_VAL210	-0.096045	-0.155373	0.059328
1	A_GLY214	-0.217391	-0.256867	0.039476
1	A_GLN215	-5.566670	-5.023760	-0.542912
1	A_CYS323	-0.022670	-0.072813	0.050144
1	A_MET324	-0.020708	-0.029367	0.008659
1	A_ILE325	-0.257601	-0.073919	-0.183682
1	A_ILE335	-1.678930	-1.693320	0.014395
1	A_THR336	-0.318276	-0.271974	-0.046302
1	A_LEU337	-1.534010	-1.495090	-0.038923
1	A_MET350	-0.821577	-0.906827	0.085250
1	A_PHE352	-2.547470	-2.435580	-0.111886
1	A_TYR407	-3.621110	-3.433030	-0.188075
1	A_THR408	0.020549	-0.028947	0.049496
1	A_GLY443	-0.146363	-0.049958	-0.096405

1	A_TYR444	-1.760950	-1.750460	-0.010495
1	A_MET445	-0.059774	-0.045053	-0.014721
1	A_FAD600	-2.649280	-2.820680	0.171401

Table 4.2. The principal interaction energies of caffeine with the active site residues and waters of MAO-B.

Name	Forcefield	Total Interaction Energy (kcal/mol)	Total VDW Interaction Energy (kcal/mol)	Total Electrostatic Interaction Energy (kcal/mol)
2V60	2V60-CHARMm	-10.86736	-11.71706	0.84970

Interaction Energies			
Residue	**Interaction Energy (kcal/mol)**	**VDW Interaction Energy (kcal/mol)**	**Electrostatic Interaction Energy (kcal/mol)**
A_TYR60	-0.073990	-0.046806	-0.027184
A_LEU88	-0.411040	-0.429793	0.018753
A_HIS90	-0.115100	-0.097951	-0.017149
A_PHE99	-0.391176	-0.252014	-0.139162
A_GLY101	-0.007357	-0.048636	0.041280
A_PRO102	-0.687786	-0.795514	0.107728
A_PHE103	-0.679071	-0.440165	-0.238906
A_PRO104	-0.487643	-0.503417	0.015774
A_HIS115	-0.068840	-0.006933	-0.061907
A_PHE118	0.005077	-0.031315	0.036393
A_TRP119	-0.545599	-0.546789	0.001190
A_LEU164	-0.448904	-0.420291	-0.028613
A_ALA165	-0.049558	-0.062515	0.012956
A_LEU167	-0.654291	-0.702782	0.048491
A_PHE168	-2.324430	-1.952790	-0.371639
A_VAL169	0.014651	-0.091207	0.105858
A_ASN170	-0.063475	-0.063031	-0.000444
A_LEU171	-2.837310	-2.740240	-0.097073
A_CYS172	-0.443868	-0.602772	0.158904
A_VAL173	-0.276434	-0.028740	-0.247694
A_THR174	0.119943	-0.009571	0.129514
A_PHE185	0.027157	-0.025582	0.052740
A_TYR188	0.046265	-0.013805	0.060069
A_VAL189	0.050785	-0.023348	0.074132
A_CYS192	0.031152	-0.005711	0.036863

A_THR195	-0.311925	-0.118359	-0.193566
A_THR196	-0.135041	-0.092614	-0.042427
A_ARG197	-0.035828	-0.067450	0.031621
A_ILE198	-1.114920	-1.126140	0.011219
A_ILE199	-7.171050	-7.097960	-0.073088
A_SER200	-0.638594	-0.621630	-0.016964
A_THR201	-0.317733	-0.318739	0.001006
A_GLY205	0.009198	-0.059991	0.069189
A_GLN206	-0.358959	-0.363584	0.004625
A_THR314	-0.383371	-0.446176	0.062805
A_ILE316	-0.526877	-0.512520	-0.014357
A_TYR326	10.787300	9.647060	1.140240
A_THR327	0.002787	-0.083747	0.086534
A_LEU328	-0.289489	-0.204535	-0.084954
A_MET341	0.036539	-0.014804	0.051343
A_PHE343	-0.022395	-0.080816	0.058420
A_TYR398	-0.200162	-0.123395	-0.076767
A_TRP432	0.028787	-0.012955	0.041742
A_TYR435	0.013801	-0.056787	0.070588
A_FAD1502	0.001626	-0.015337	0.016963
A_HOH1309	0.029790	-0.004865	0.034655

Since caffeine mapped to the structure-based pharmacophore model of MAO-A, the orientation of caffeine within this model is given below. As shown caffeine fits the shape of the pharmacophore and maps to two hydrophobic features (cyan spheres) and one acceptor feature (green sphere). The acceptor feature corresponds to the carbonyl oxygen at C6 of the caffeine ring, while the hydrophobic features correspond to the methyl groups on N3 and N7 of the caffeine ring.

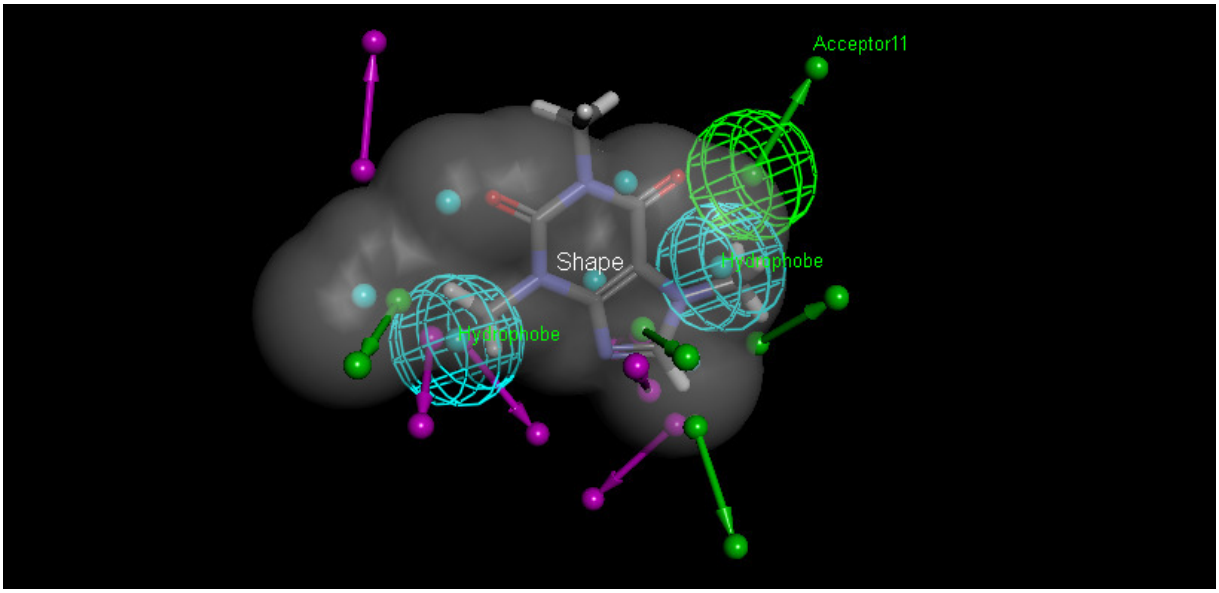

Figure 4.47. The orientation of caffeine in the MAO-A structure-based pharmacophore model.

4.5.4. Dantroline

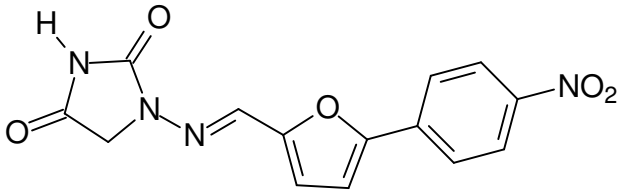

Figure 4.48. The structure of dantroline.

The structure of dantroline is given above. Dantroline is a direct-acting skeletal muscle relaxant. It inhibits contraction induced by electrical stimulation, acetylcholine and potassium in skeletal muscle (Nasu *et al*., 1996). It is clinically used for muscle spasticity and malignant hyperthermia (Li *et al*., 2005). The results of the MAO inhibition studies show that dantroline is an inhibitor of both MAO-A and MAO-B. The concentration-response curves of the MAO-A and MAO-B catalytic activities in presence of increasing concentrations of dantroline are given below. The graph shows that there is a significant decrease in the catalytic activities of MAO-A and MAO-B with increasing

concentrations of dantroline. Maximal suppression of MAO-A and MAO-B activities were, however, not achieved with the maximal concentration tested 100 µM. The IC_{50} values recorded for the inhibition of MAO-A and MAO-B are estimated at 42.8 ± 3.8 µM and 9.2 ± 0.9 µM, respectively.

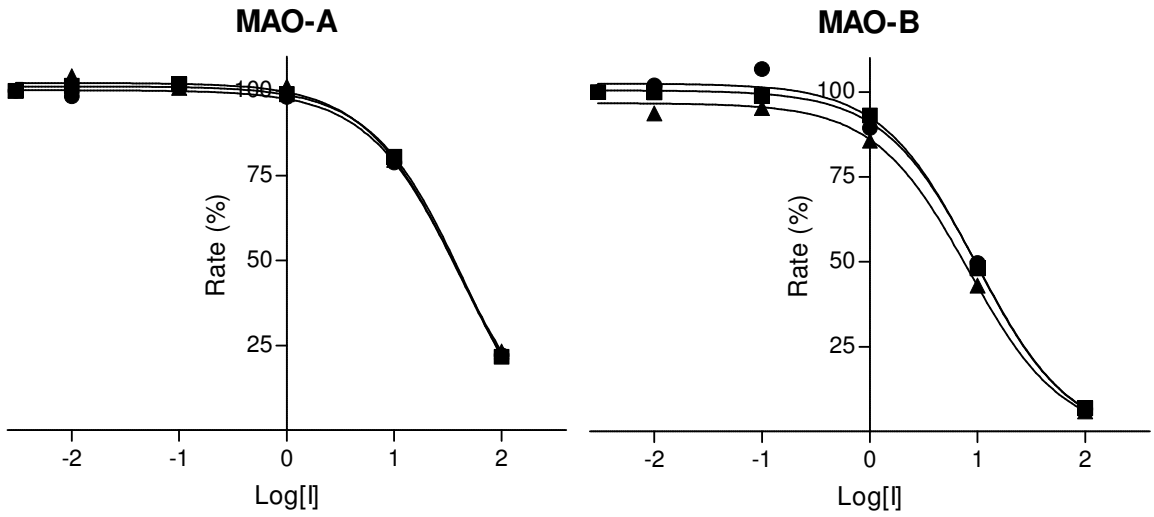

Figure 4.49. The recombinant human MAO-A (left) and MAO-B (right) catalyzed oxidation of kynuramine in the presence of various concentrations of dantroline (expressed in µM). The concentration-response curves were constructed from the initial rates of kynuramine oxidation versus the logarithm of the concentration of dantroline. The rates are expressed as the percentage of the catalytic rate recorded in the absence of inhibitor.

4.5.5. Esomeprazole

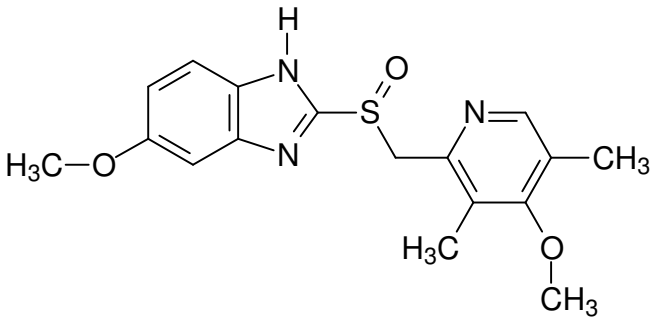

Figure 4.50. The structure of esomeprazole.

The structure of esomeprazole is given above. Esomeprazole, a benzimidazole compound, is a gastric parietal cell proton pump inhibitor which is widely used for the treatment of acid-related gastric diseases, because it inhibits acid secretion (Gisbert & Pajares., 2004). It is used in the treatment of peptic ulcer disease and gastro-eosophageal reflux. The results of the MAO inhibition studies show that esomeprazole is an inhibitor of both MAO-A and MAO-B with IC_{50} values of 23.2 ± 1.51 µM and 48.3 ± 3.08 µM, respectively. The concentration-response curves of the MAO-A and MAO-B catalytic activity in presence of increasing concentrations of esomeprazole are given below. The graph shows that there is a decrease in the catalytic activities of both MAO-A and MAO-B with increasing concentrations of esomeprazole. Based on its relatively good MAO inhibition potencies, the interactions of esomeprazole with these enzymes were thus further investigated. The interactions of esomeprazole with the MAOs will be further analyzed in Chapter 5 where these results will be presented as an article.

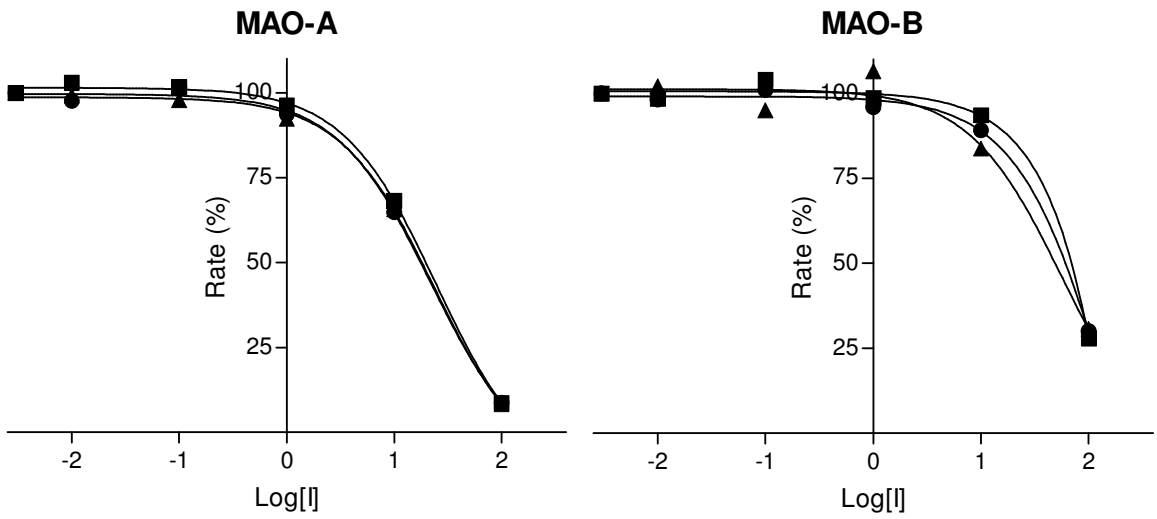

Figure 4.51. The recombinant human MAO-A (left) and MAO-B (right) catalyzed oxidation of kynuramine in the presence of various concentrations of esomeprazole (expressed in µM). The concentration-response curves were constructed from the initial rates of kynuramine oxidation versus the logarithm of the concentration of esomeprazole. The rates are expressed as the percentage of the catalytic rate recorded in the absence of inhibitor.

The reversibility of the interaction of esomeprazole with MAO-A and MAO-B were further investigated by evaluating the recovery of the enzymatic activity after dilution of the enzyme-inhibitor complexes. For this purpose, MAO-A and MAO-B were preincubated with esomeprazole at concentrations of 10 × IC_{50} and 100 × IC_{50} for 30 min. The reactions were subsequently diluted 100-fold to 0.1 × IC_{50} and 1 × IC_{50}, respectively. The results are given in figure 4.52 and show that after diluting the MAO-esomeprazole complexes to concentrations equal to 0.1 × IC_{50}, the MAO-A and MAO-B activities were recovered to levels of 94% and 87% of the control values, respectively. This behaviour is consistent with a reversible interaction of esomeprazole with MAO-A and MAO-B. For reversible inhibition, dilution of the enzyme-inhibitor complex to an inhibitor concentration of 0.1 × IC_{50} is expected to result in approximately 90% recovery in enzyme activity. In contrast, after similar treatment of MAO-A and MAO-B with the irreversible inhibitors pargyline and (R)-deprenyl, respectively, the MAO-A and MAO-B

activities were not recovered. Pargyline and (R)-deprenyl, at concentrations of 10 × IC_{50}, were preincubated with MAO-A and MAO-B, respectively, and the resulting enzyme-inhibitor complexes were diluted 100-fold to yield inhibitor concentrations of 0.1 × IC_{50}. As shown in figure 4.52, after dilution the enzyme activities are only 1.2% and 3.4% of the control values recorded in absence of inhibitor.

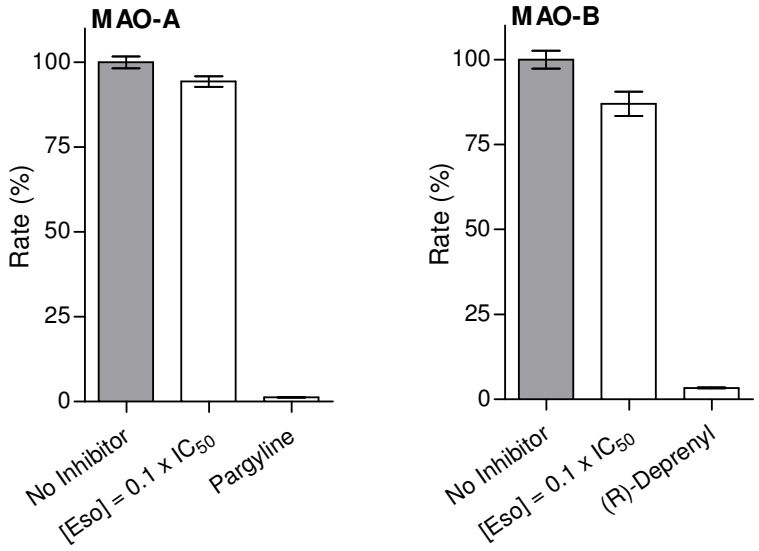

Figure 4.52. Reversibility of inhibition of MAO-A (left) and MAO-B (right) by esomeprazole. The enzyme was preincubated with the test inhibitor at 10 × IC_{50} and 100 × IC_{50} for 30 min and then diluted to 0.1 × IC_{50} and 1 × IC_{50}, respectively. As controls, MAO-A and MAO-B were also preincubated with pargyline and (R)-deprenyl, respectively, at 10 × IC_{50} and subsequently diluted to 0.1 × IC_{50}. The residual enzyme activities were subsequently measured.

The reversibility of MAO-A and MAO-B inhibition by esomeprazole was also investigated by measuring the recoveries of enzyme activities after dialysis of enzyme-inhibitor mixtures (Harfenist *et al*., 1996). The MAO enzymes and esomeprazole, at a concentration of 4 × IC_{50}, were preincubated for a period of 15 min and subsequently dialyzed for 24 h. The results, given in Fig. 4.53, show that MAO-A and MAO-B inhibition by esomeprazole is almost completely reversed after 24 h of dialysis with the MAO-A and MAO-B activities recovering to levels of 93% and 88% of the control values, respectively. In contrast, the MAO-A and MAO-B activities in undialyzed mixtures of the

enzymes with esomeprazole are 24% and 26%, respectively, of the control values. This behaviour is consistent with a reversible interaction between the MAO enzymes and esomeprazole. For comparison, after similar preincubation and dialysis of MAO-A and MAO-B with the irreversible inhibitors, pargyline and (R)-deprenyl, respectively, the enzyme activities are not recovered. After dialysis of MAO-A–pargyline and MAO-B–(R)-deprenyl mixtures, the residual enzyme activities are recovered to levels of only 1.2% and 4.2%, respectively, of the control values.

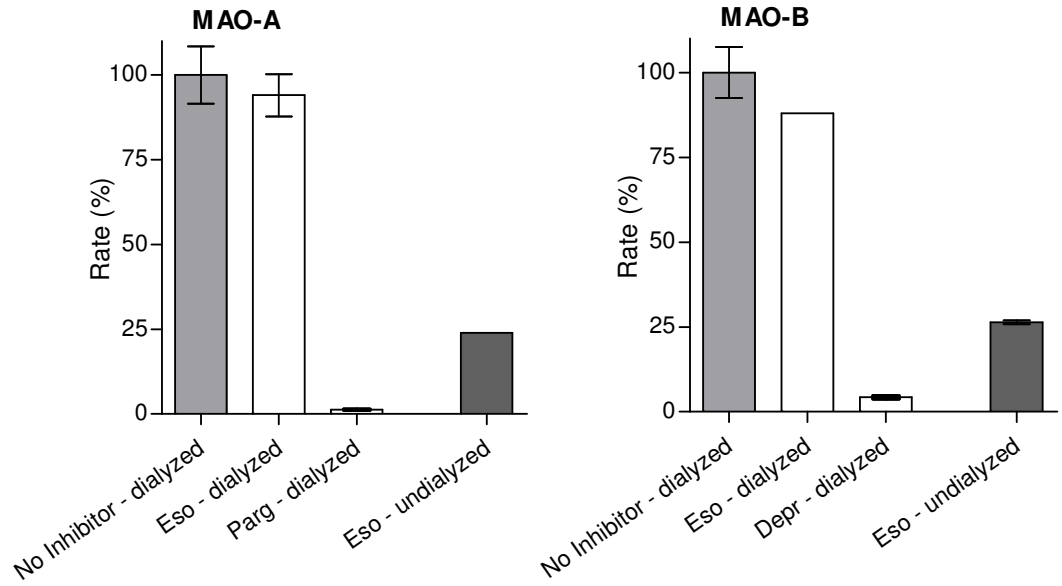

Figure 4.53. Reversibility of inhibition of MAO-A (left) and MAO-B (right) by esomeprazole. The MAO enzymes and esomeprazole, at a concentration of 4 × IC_{50}, were preincubated for a period of 15 min, dialyzed for 24 h and the residual enzyme activities were subsequently measured (Eso–dialyzed). For comparison, the MAOs were similarly preincubated in the absence (No inhibitor–dialyzed) and presence of the irreversible inhibitors, pargyline (Parg–dialyzed) and (R)-deprenyl (Depr–dialyzed), respectively, and dialyzed. The residual MAO activities of undialyzed mixtures (Eso–undialyzed) of the MAOs with esomeprazole are also shown.

The modes of MAO-A and MAO-B inhibition by esomeprazole were investigated by constructing a set of Lineweaver–Burk plots for the inhibition of MAO-A and MAO-B. The catalytic rates were measured in the presence of three different concentrations of esomeprazole, and in the absence of esomeprazole. These measurements were carried out using four different concentrations of the substrate, kynuramine (15–90 µM). Figure 4.54 illustrates the set of Lineweaver–Burk plots that were obtained from these studies. The results show that the Lineweaver–Burk plots for the inhibition of both MAO-A and MAO-B, are linear and intersect at a single point. From these data it may be concluded that esomeprazole most likely interacts competitively and therefore reversibly with both enzymes.

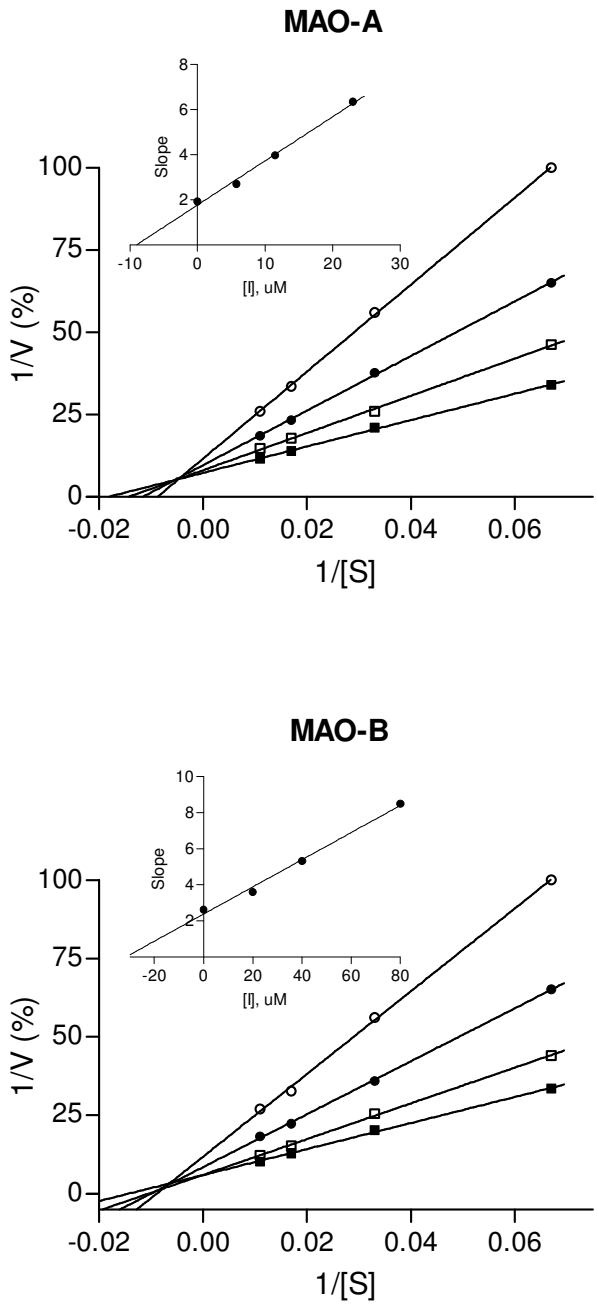

Figure 4.54. Lineweaver-Burk plots of the oxidation of kynuramine by recombinant human MAO-A (top) and MAO-B (bottom). The plots were constructed in the absence (filled squares) and presence of various concentrations of esomeprazole. The concentrations of esomeprazole employed were ¼ × IC_{50} (open squares), ½ × IC_{50} (filled circles) and 1 × IC_{50} (open circles), respectively.

To provide additional insight, the binding modes of esomeprazole within the active site cavities of MAO-A and MAO-B were examined. The molecular docking simulations were carried out according to the protocol given in Chapter 2. The results are given in figure 4.55 and tables 4.4 and 4.5. As shown in the three-dimensional representations, in the MAO-A active site, esomeprazole undergoes hydrogen bonding with Cys323, the phenolic hydrogen of Tyr407 and the FAD cofactor. Of these interactions, only that to the FAD cofactor (–3.43 kcal/mol) contributes to the binding. The interactions with Cys323 and Tyr407 are non-productive with interaction energies of +637 kcal/mol and 18.9 kcal/mol, respectively. In fact, esomeprazole also undergoes non-productive interactions with Phe208, Leu337 and Phe352. These unfavorable interactions suggest that esomeprazole should not be able to bind to MAO-A. The experimental results, however, shows that esomeprazole is a MAO-A inhibitor. This suggests that induced fit may occur to better accommodate this inhibitor in the MAO-A active site. These results suggest that molecular docking may not be appropriate to determine if compounds bind to MAO-A and alternative methods such as pharmacophore screening used in this study may be more effective. Significant interactions (hydrophobic) occur between esomeprazole and Tyr69, Ile180, and Gln215. The interaction energies show that these amino acid residues contribute significantly to the total binding energy of the ligand (–2.22, –3.22, –4.31 kcal/mol, respectively).

In the MAO-B active site, esomeprazole undergoes hydrogen bonding with Cys172. The interaction energy of this interaction contributes to the total binding energy (–1.98 kcal/mol). Esomeprazole also undergoes π-π interactions with Tyr398 and Tyr435. The contributions of these interactions to the binding energy of the inhibitor are substantial with interaction energies of –3.76 kcal/mol and –2.75 kcal/mol, respectively. This finding is in accordance to literature which reports that MAO substrates binds between Tyr398 and Tyr435 and are thus stabilized (Binda *et al*., 2003). Significant interactions (hydrophobic) also occur between esomeprazole and Tyr60 (–1.53 kcal/mol), Phe168 (–2.53 kcal/mol), Leu171 (–2.95 kcal/mol), Ile199 (–4.70 kcal/mol), Gln206 (–3.37 kcal/mol) and the FAD cofactor (–4.71 kcal/mol). Based on the more negative energies, the interactions with Ile199 and the FAD cofactor are especially important.

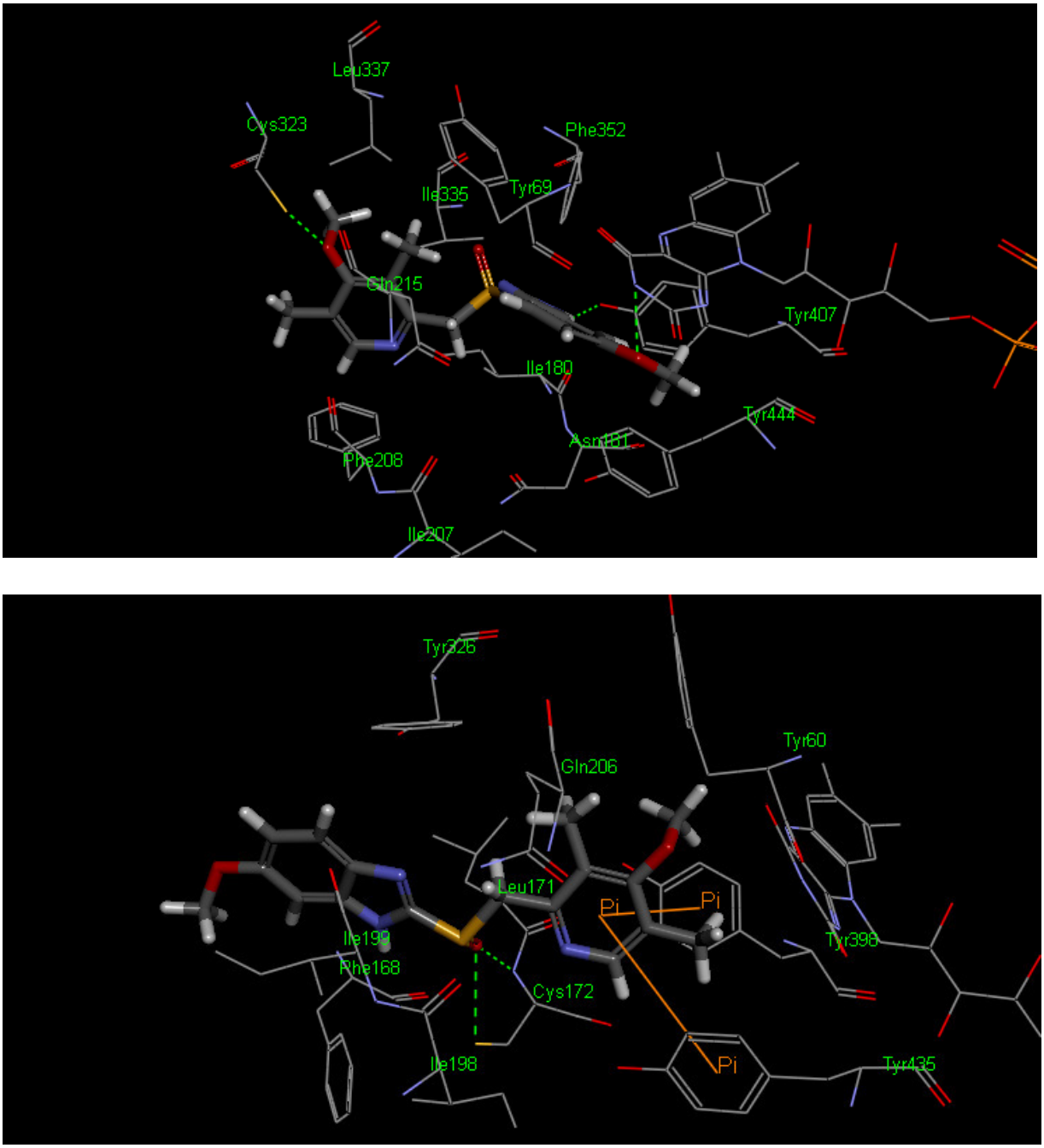

Figure 4.55. The docked orientations of esomeprazole within the MAO-A (top) and MAO-B (bottom) active sites.

Table 4.3. The principal interaction energies of esomeprazole with the active site residues and waters of MAO-A.

Name	Forcefield	Total Interaction Energy (kcal/mol)	Total VDW Interaction Energy (kcal/mol)	Total Electrostatic Interaction Energy (kcal/mol)
2Z5X	2Z5X-CHARMm	729.17542	732.35492	-3.17950

Interaction Energies			
Residue	**Interaction Energy (kcal/mol)**	**VDW Interaction Energy (kcal/mol)**	**Electrostatic Interaction Energy (kcal/mol)**
A_TYR69	-2.219980	-2.337700	0.117716
A_VAL70	-0.158634	-0.141198	-0.017436
A_GLN74	-0.178894	-0.152778	-0.026116
A_VAL91	-0.083771	-0.153036	0.069265
A_VAL93	-0.119025	-0.123815	0.004790
A_LEU97	-1.048010	-1.121880	0.073867
A_PHE108	-0.108562	-0.158346	0.049784
A_ALA111	-0.654784	-0.494082	-0.160702
A_PHE112	-0.239597	-0.182344	-0.057253
A_ILE180	-3.221200	-2.717840	-0.503358
A_ASN181	-0.802887	-0.742254	-0.060633
A_THR183	-0.069877	-0.150573	0.080696
A_TYR197	-0.530379	-0.448466	-0.081913
A_ILE207	-0.534481	-0.566659	0.032178
A_PHE208	5.797570	6.457930	-0.660363
A_SER209	-0.580875	-0.598666	0.017791
A_VAL210	-1.473910	-1.406390	-0.067524
A_GLY214	-0.730933	-0.651672	-0.079261
A_GLN215	-4.308390	-4.086350	-0.222036
A_CYS323	636.943970	637.755005	-0.811451
A_MET324	-0.300080	-0.400504	0.100424
A_ILE325	-1.591750	-1.530530	-0.061225
A_ILE335	-4.934320	-4.962240	0.027919
A_THR336	-0.514177	-0.030506	-0.483671
A_LEU337	94.779404	94.862297	-0.082867
A_MET350	-0.631412	-0.737968	0.106556
A_PHE352	3.008900	2.921290	0.087611
A_TYR407	18.923000	18.796801	0.126214
A_THR408	-0.149354	-0.149900	0.000546
A_GLY443	-0.424053	-0.150653	-0.273400

A_TYR444	-1.052280	-0.802619	-0.249657
A_MET445	-0.182716	-0.237928	0.055212
A_FAD600	-3.432410	-3.201200	-0.231205

Table 4.4. The principal interaction energies of esomeprazole with the active site residues and waters of MAO-B.

Name	Forcefield	Total Interaction Energy (kcal/mol)	Total VDW Interaction Energy (kcal/mol)	Total Electrostatic Interaction Energy (kcal/mol)
2V60	2V60-CHARMm	-44.2771	-43.337	-0.9373

Interaction Energies			
Residue	**Interaction Energy (kcal/mol)**	**VDW Interaction Energy (kcal/mol)**	**Electrostatic Interaction Energy (kcal/mol)**
A_TYR60	-1.537610	-1.530930	-0.006677
A_LEU88	-0.121592	-0.112105	-0.009487
A_HIS90	-0.171356	-0.124015	-0.047341
A_PHE99	-0.187250	-0.149080	-0.038170
A_GLY101	0.022900	-0.025972	0.048872
A_PRO102	-0.532195	-0.481681	-0.050514
A_PHE103	-0.891918	-0.697663	-0.194255
A_PRO104	-0.973944	-0.985339	0.011395
A_HIS115	0.045422	-0.028010	0.073433
A_PHE118	-0.004637	-0.058459	0.053822
A_TRP119	0.839238	0.652790	0.186448
A_LEU164	-1.480840	-1.397960	-0.082879
A_ALA165	-0.035167	-0.092472	0.057306
A_LEU167	-0.752113	-0.734825	-0.017288
A_PHE168	-2.532700	-2.868730	0.336033
A_VAL169	-0.185164	-0.162170	-0.022994
A_ASN170	-0.279513	-0.139009	-0.140504
A_LEU171	-2.951420	-2.770520	-0.180896
A_CYS172	-1.978750	-1.885340	-0.093413
A_VAL173	-0.363166	-0.232993	-0.130173
A_THR174	-0.023100	-0.141954	0.118854
A_PHE185	0.007827	-0.057659	0.065486
A_TYR188	-0.480941	-0.319219	-0.161722
A_VAL189	-0.117498	-0.055425	-0.062072
A_CYS192	-0.127289	-0.049400	-0.077888

A_THR195	-0.046688	-0.135506	0.088818
A_THR196	-0.069945	-0.088244	0.018298
A_ARG197	-0.083312	-0.084690	0.001378
A_ILE198	-1.704270	-1.849340	0.145072
A_ILE199	-4.700120	-4.426990	-0.273125
A_SER200	-0.444671	-0.388346	-0.056325
A_THR201	-0.057247	-0.148682	0.091435
A_GLY205	-0.249296	-0.235336	-0.013960
A_GLN206	-3.366160	-3.353120	-0.013043
A_THR314	-0.155439	-0.119229	-0.036210
A_ILE316	-1.885600	-1.880080	-0.005520
A_TYR326	-3.295740	-3.085500	-0.210235
A_THR327	0.147598	-0.070107	0.217705
A_LEU328	-0.401612	-0.363816	-0.037796
A_MET341	-0.252878	-0.180597	-0.072281
A_PHE343	-1.566350	-1.622540	0.056194
A_TYR398	-3.755440	-3.372330	-0.383112
A_TRP432	-0.098883	-0.147102	0.048219
A_TYR435	-2.753610	-2.424570	-0.329039
A_FAD1502	-4.717160	-4.907990	0.190830

Since esomeprazole mapped to the structure-based pharmacophore model of MAO-B, the orientation of esomeprazole within this model is given below. As shown, esomeprazole fits the shape of the pharmacophore and maps to two hydrophobic features (cyan spheres) and one acceptor feature (green sphere). The acceptor feature corresponds to the methoxy oxygen on the benzimidazole ring, while the hydrophobic features correspond to the methyl and methoxy groups on pyridine ring of the drug.

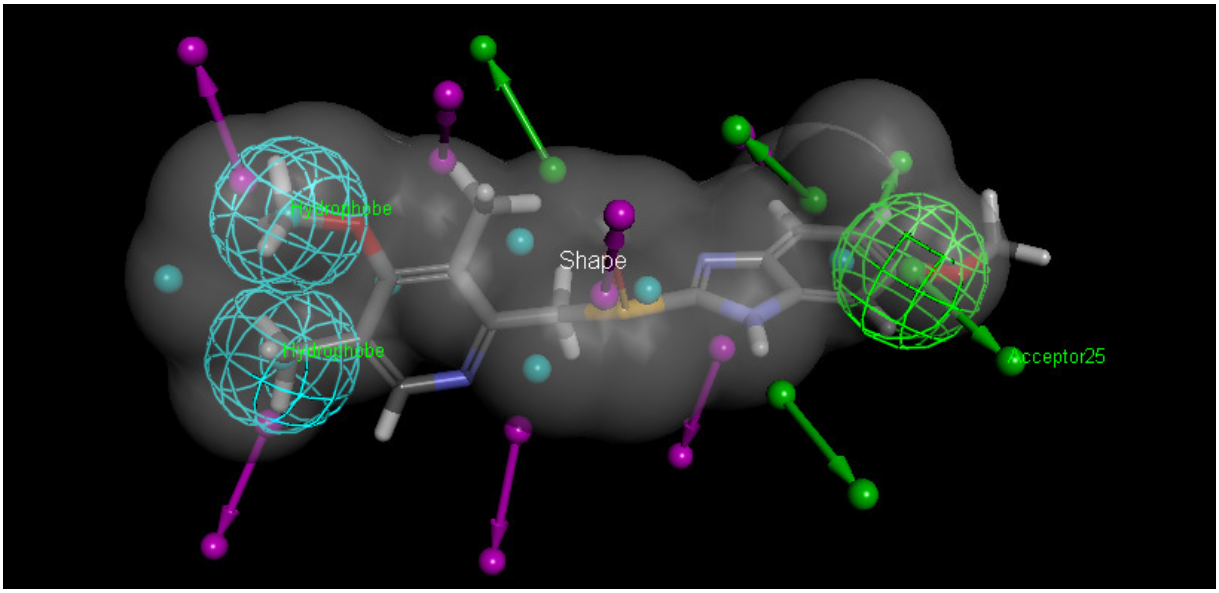

Figure 4.56. The orientation of esomeprazole in the MAO-B structure-based pharmacophore model.

4.5.6. Ethoxzolamide

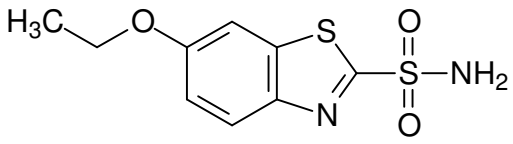

Figure 4.57. The structure of ethoxzolamide.

The structure of ethoxzolamide is given above. Ethoxzolamide is a sulfonamide which inhibits carbonic anhydrase. It may be used as a diuretic and in the treatment of diseases including glaucoma and ulcers (Innocenti *et al*., 2005). The results of the MAO inhibition studies show that ethoxzolamide is an inhibitor of MAO-B. Ethoxzolamide is a very weak inhibitor of MAO-A at maximal tested concentration of 100 μM. The concentration-response curves of the MAO-A and MAO-B catalytic activity in presence of increasing concentrations of ethoxzolamide are given below. The graph shows that there is only a small decrease in the catalytic activity of MAO-A with increasing concentrations of ethoxzolamide. There is, however, a significant decrease in the catalytic activity of MAO-B with increasing concentrations of ethoxzolamide. Maximal

suppression of MAO-B activity was, however, not achieved with the maximal concentration tested 100 µM. The IC_{50} values recorded for the inhibition of MAO-A and MAO-B are estimated at 174.3 ± 14.3 µM and 64.1 ± 16.1 µM, respectively.

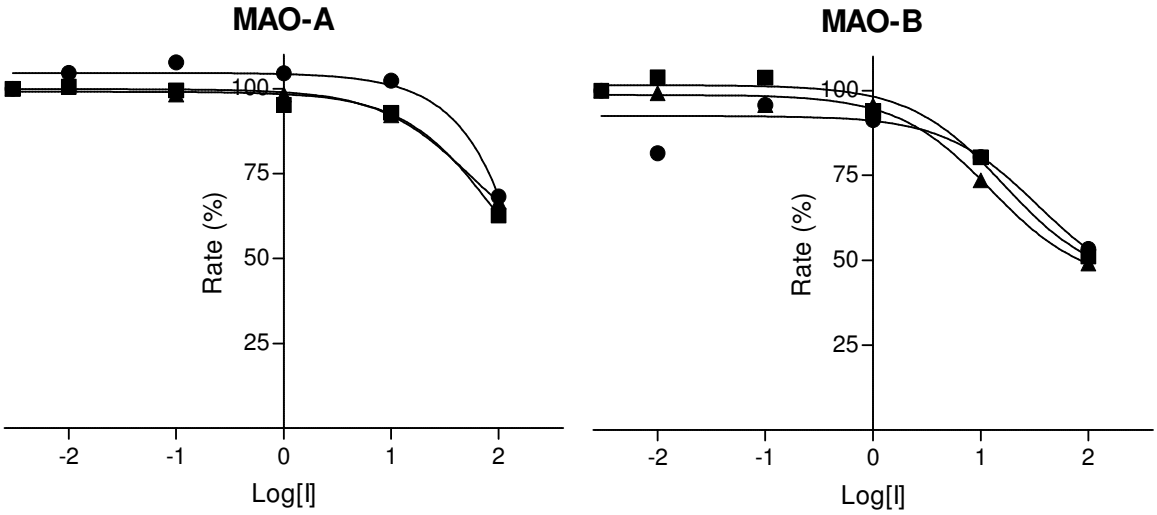

Figure 4.58. The recombinant human MAO-A (left) and MAO-B (right) catalyzed oxidation of kynuramine in the presence of various concentrations of ethoxzolamide (expressed in µM). The concentration-response curves were constructed from the initial rates of kynuramine oxidation versus the logarithm of the concentration of ethoxzolamide. The rates are expressed as the percentage of the catalytic rate recorded in the absence of inhibitor.

4.5.7. Hesperetin

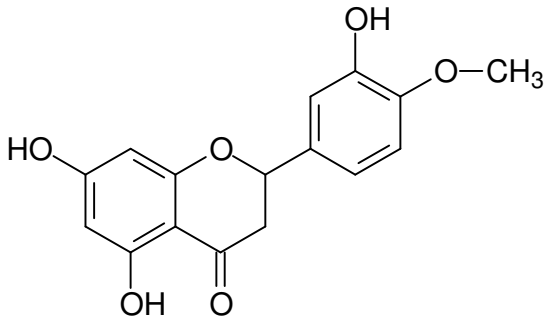

Figure 4.59. The structure of hesperetin.

The structure of hesperetin is given above. Hesperetin is a natural compound found in citrus fruits. It has anti-cancer activity by inhibiting proliferation or inducing apoptosis, inhibiting angiogenesis and by acting as an anti-oxidant (Yang *et al*., 2012). It also has anti-oxidant properties, it may increase the ocular blood flow and minimize ischemic injury to the retina. Hesperetin may also decrease vascular permeability and act as neuroprotectant (Srirangam & Saoumyajit, 2010). The results of the MAO inhibition studies show that hesperetin is an inhibitor of both MAO-A and MAO-B. The concentration-response curves of the MAO-A and MAO-B catalytic activity in presence of increasing concentrations of hesperetin are given below. The graph shows that there is a significant decrease in the catalytic activities of MAO-A and MAO-B with increasing concentrations of hesperetin. Maximal suppression of MAO-A and MAO-B activities were, however, not achieved with the maximal concentration tested 100 µM. The IC_{50} values recorded for the inhibition of MAO-A and MAO-B are estimated at 48.4 ± 1.9 µM and 32.9 ± 2.9 µM, respectively.

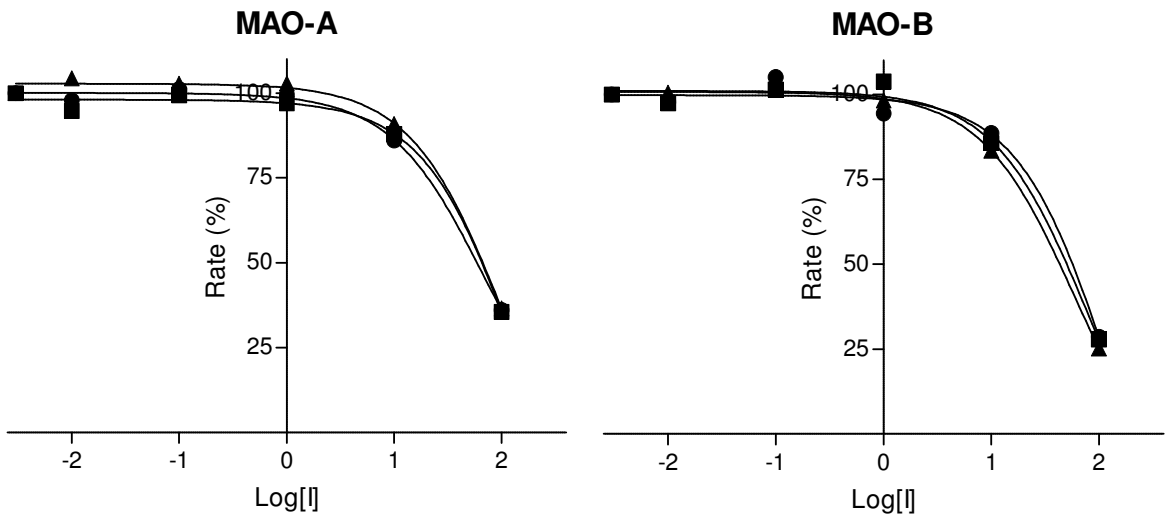

Figure 4.60. The recombinant human MAO-A (left) and MAO-B (right) catalyzed oxidation of kynuramine in the presence of various concentrations of hesperetin (expressed in μM). The concentration-response curves were constructed from the initial rates of kynuramine oxidation versus the logarithm of the concentration of hesperetin. The rates are expressed as the percentage of the catalytic rate recorded in the absence of inhibitor.

4.5.8. Leflunomide

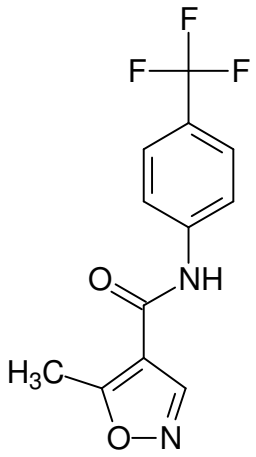

Figure 4.61. The structure of leflunomide.

The structure of leflunomide is given. Leflunomide is an isoxazole derivative and a disease modifying antirheumatic drug for the treatment of rheumatoid arthritis (Boyd, 2012). Leflunomide is a pro-drug with its metabolite, a malononitrilamide termed A77-1726, acting as the active drug. Leflunomide is absorbed from the gastro-intestinal tract and undergoes first pass metabolism in the gut wall, liver and possibly the plasma (Rozman, 2002). The absorption of leflunomide is influenced by the presence of food and the relative bioavailability of a 10 mg formulation is 94%, in terms of plasma concentration of A77-1726 (Rozman, 2002). After oral administration 95% leflunomide is converted to A77-1726. Protein binding of A77-1726 is 99.38%. Leflunomide undergoes renal and faecal elimination. The biotransformation of leflunomide to its metabolite A77-1726 is given in the structure below.

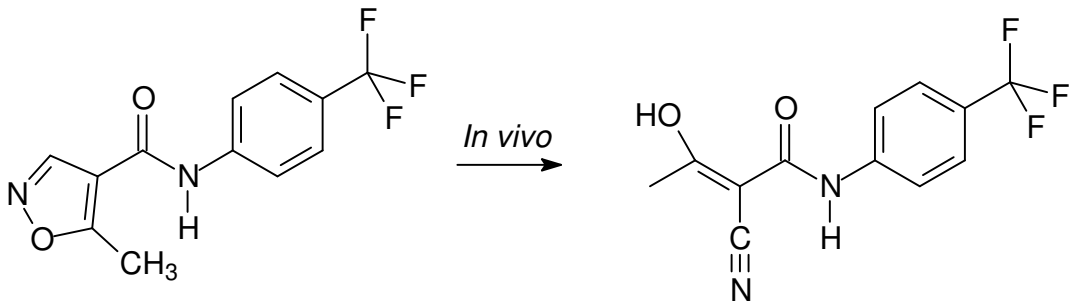

Leflunomide A77-1726

Figure 4.62. Biotransformation of leflunomide to A77-1726.

The results of the MAO inhibition studies show that leflunomide is an inhibitor of both MAO-A and MAO-B with IC_{50} values of 19.1 ± 2.55 µM and 13.7 ± 0.752 µM, respectively. The concentration-response curves of the MAO-A and MAO-B catalytic activity in presence of increasing concentrations of leflunomide are given below. The graph shows that there is a decrease in the catalytic activities of both MAO-A and MAO-B with increasing concentrations of leflunomide.

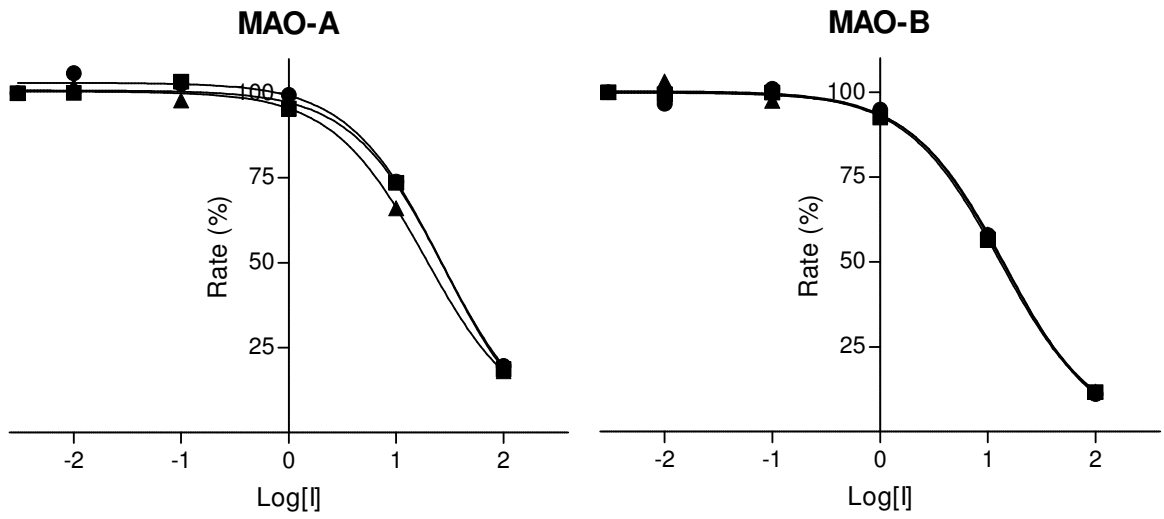

Figure 4.63. The recombinant human MAO-A (left) and MAO-B (right) catalyzed oxidation of kynuramine in the presence of various concentrations of leflunomide (expressed in μM). The concentration-response curves were constructed from the initial rates of kynuramine oxidation versus the logarithm of the concentration of leflunomide. The rates are expressed as the percentage of the catalytic rate recorded in the absence of inhibitor.

To provide additional insight, the binding modes of leflunomide within the active site cavities of MAO-A and MAO-B were examined. The molecular docking simulations were carried out according to the protocol given in Chapter 2. The results are given in figure 4.64 and tables 4.5 and 4.6. As shown in the three-dimensional representations, in the MAO-A active site, leflunomide undergoes hydrogen bonding with Cys323 and the phenolic hydrogen of Tyr444. Leflunomide also undergoes π-π interactions with Tyr444. The interaction with Tyr444 (–1.96 kcal/mol) represents a productive interaction while the interaction with Cys323 is non-productive with an interaction energy of +5.19 kcal/mol. Significant interactions (hydrophobic) occur between leflunomide and Ile180 (–3.36 kcal/mol), Ile207 (–1.98 kcal/mol), Phe208 (–3.65 kcal/mol), Gln215 (–2.36 kcal/mol), Ile335 (–2.61 kcal/mol), Leu337 (–2.14 kcal/mol), Tyr407 (–2.63 kcal/mol) and the FAD cofactor (–2.84 kcal/mol). The interaction energies show that these amino acid residues (and the FAD) contribute significantly to the total binding energy of the ligand.

In the MAO-B active site, leflunomide does not undergo hydrogen bonding or π-π interactions. Significant interactions (hydrophobic), however, also occur between leflunomide and Phe186 (–2.68 kcal/mol), Leu171 (–3.70 kcal/mol), Ile198 (–2.14 kcal/mol), Ile199 (–5.60 kcal/mol) and Tyr326 (–3.38 kcal/mol). Based on the more negative energies, the interaction with Ile199 is especially important.

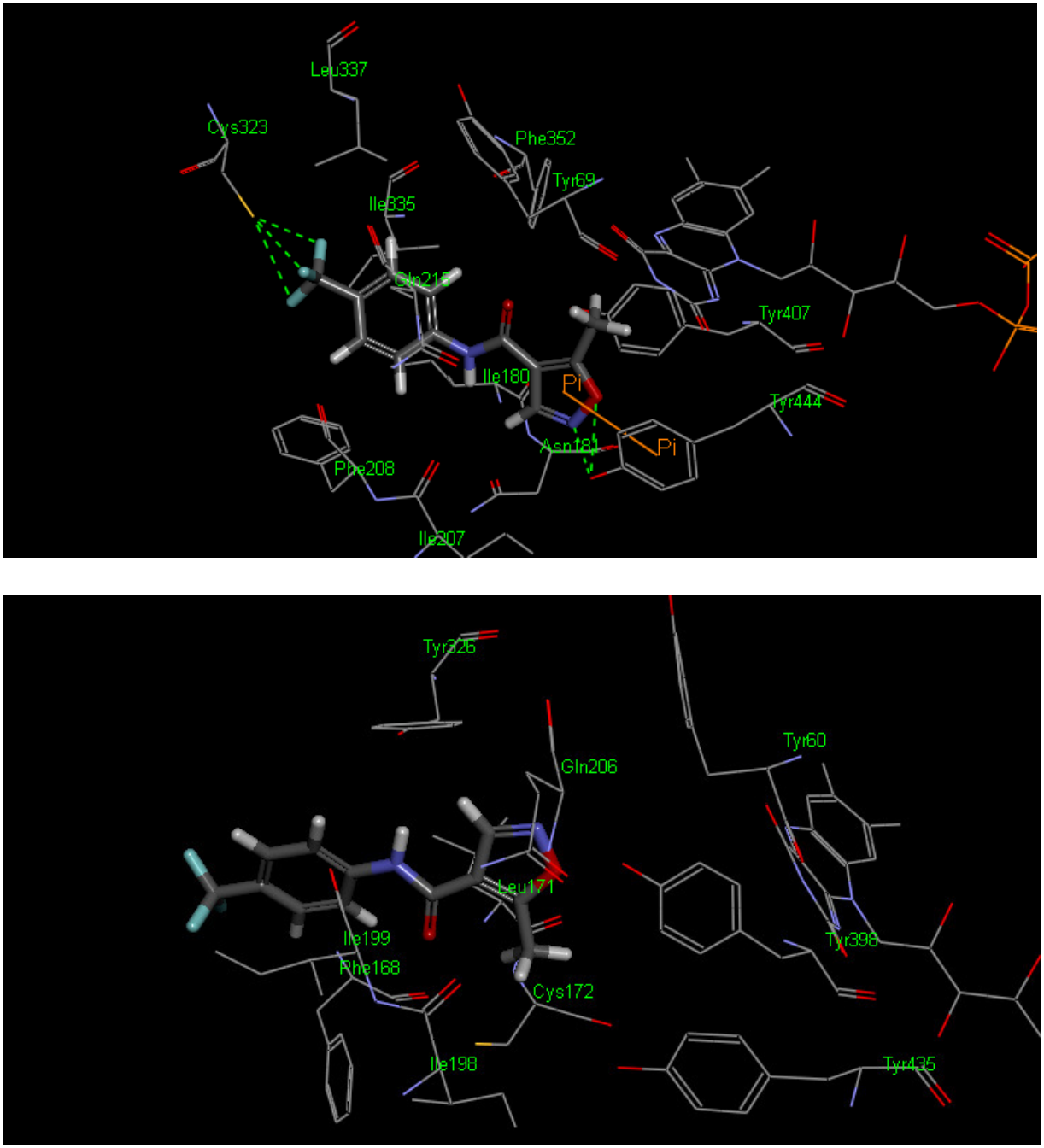

Figure 4.64. The docked orientations of leflunomide within the MAO-A (top) and MAO-B (bottom) active sites.

Table 4.5. The principal interaction energies of leflunomide with the active site residues of MAO-A.

Name	Forcefield	Total Interaction Energy (kcal/mol)	Total VDW Interaction Energy (kcal/mol)	Total Electrostatic Interaction Energy (kcal/mol)
2Z5X	2Z5X-CHARMm	-27.39763	-25.60088	-1.79675

Interaction Energies			
Residue	**Interaction Energy (kcal/mol)**	**VDW Interaction Energy (kcal/mol)**	**Electrostatic Interaction Energy (kcal/mol)**
A_TYR69	-0.906969	-0.751634	-0.155335
A_VAL70	0.078587	-0.036551	0.115138
A_GLN74	-0.042921	-0.044255	0.001334
A_VAL91	-0.114616	-0.082416	-0.032201
A_VAL93	-0.077974	-0.068310	-0.009665
A_LEU97	-0.320600	-0.335795	0.015195
A_PHE108	-0.092237	-0.050526	-0.041711
A_ALA111	-0.203833	-0.121736	-0.082097
A_PHE112	-0.094297	-0.079379	-0.014918
A_ILE180	-3.355440	-3.242550	-0.112887
A_ASN181	-1.266950	-0.427615	-0.839338
A_THR183	-0.024374	-0.136318	0.111944
A_TYR197	-0.619883	-0.428202	-0.191681
A_ILE207	-1.978210	-1.551150	-0.427062
A_PHE208	-3.647320	-3.324060	-0.323257
A_SER209	-0.577948	-0.476322	-0.101626
A_VAL210	-0.929326	-0.872678	-0.056648
A_GLY214	-0.210045	-0.248936	0.038891
A_GLN215	-2.357240	-2.295350	-0.061886
A_CYS323	5.190690	5.072880	0.117812
A_MET324	-0.235884	-0.201426	-0.034458
A_ILE325	-0.731952	-0.752261	0.020309
A_ILE335	-2.610450	-2.563840	-0.046610
A_THR336	-0.505569	-0.715392	0.209823
A_LEU337	-2.137570	-2.027220	-0.110352
A_MET350	-0.454980	-0.337733	-0.117247
A_PHE352	-1.538880	-1.407550	-0.131332
A_TYR407	-2.629820	-2.856840	0.227020
A_THR408	-0.043237	-0.059064	0.015827
A_GLY443	-0.135665	-0.099028	-0.036637

A_TYR444	-1.956720	-2.145170	0.188445
A_MET445	-0.023552	-0.053351	0.029799
A_FAD600	-2.842440	-2.881100	0.038660

Table 4.6. The principal interaction energies of leflunomide with the active site residues and waters of MAO-B.

Name	Forcefield	Total Interaction Energy (kcal/mol)	Total VDW Interaction Energy (kcal/mol)	Total Electrostatic Interaction Energy (kcal/mol)
2V60	2V60-CHARMm	-32.15139	-31.18532	-0.96607

Interaction Energies			
Residue	**Interaction Energy (kcal/mol)**	**VDW Interaction Energy (kcal/mol)**	**Electrostatic Interaction Energy (kcal/mol)**
A_TYR60	-0.265251	-0.208204	-0.057047
A_LEU88	0.086203	-0.096630	0.182833
A_HIS90	-0.354155	-0.161881	-0.192274
A_PHE99	-0.130738	-0.159059	0.028321
A_GLY101	-0.089667	-0.026569	-0.063098
A_PRO102	-0.666167	-0.525570	-0.140597
A_PHE103	-1.062970	-0.949157	-0.113812
A_PRO104	-1.119990	-1.081660	-0.038330
A_HIS115	-0.163448	-0.033850	-0.129598
A_PHE118	-0.030527	-0.068913	0.038386
A_TRP119	-0.196275	-0.239850	0.043575
A_LEU164	-1.517620	-1.470770	-0.046854
A_ALA165	-0.060431	-0.113972	0.053541
A_LEU167	-0.844981	-0.830501	-0.014480
A_PHE168	-2.684150	-2.771130	0.086983
A_VAL169	-0.073996	-0.127370	0.053374
A_ASN170	-0.003653	-0.095811	0.092158
A_LEU171	-3.704480	-3.649500	-0.054978
A_CYS172	-1.207110	-1.395250	0.188141
A_VAL173	-0.087040	-0.099284	0.012244
A_THR174	-0.112076	-0.039877	-0.072199
A_PHE185	0.069726	-0.042641	0.112367
A_TYR188	-0.079875	-0.078017	-0.001858
A_VAL189	-0.050562	-0.043822	-0.006740
A_CYS192	-0.092352	-0.022955	-0.069397

A_THR195	-0.042353	-0.146058	0.103705
A_THR196	0.056023	-0.096992	0.153015
A_ARG197	-0.194266	-0.084239	-0.110027
A_ILE198	-2.145800	-1.998160	-0.147644
A_ILE199	-5.600070	-5.127250	-0.472821
A_SER200	-0.422931	-0.406215	-0.016716
A_THR201	-0.394702	-0.153155	-0.241547
A_GLY205	-0.157447	-0.127504	-0.029943
A_GLN206	-1.673970	-2.036900	0.362932
A_THR314	0.103762	-0.108017	0.211779
A_ILE316	-1.684280	-1.805070	0.120790
A_TYR326	-3.377240	-2.529760	-0.847480
A_THR327	-0.144444	-0.067286	-0.077158
A_LEU328	-0.177640	-0.272147	0.094507
A_MET341	-0.146212	-0.047014	-0.099197
A_PHE343	-0.349818	-0.316722	-0.033096
A_TYR398	-0.826314	-0.851305	0.024991
A_TRP432	-0.043988	-0.049136	0.005148
A_TYR435	-0.416747	-0.438625	0.021878
A_FAD1502	-0.037941	-0.147164	0.109223
A_HOH1309	-0.033417	-0.044345	0.010927

Since leflunomide mapped to the structure-based pharmacophore model of MAO-B, the orientation of leflunomide within this model is given below. As shown, leflunomide fits the shape of the pharmacophore and maps to two hydrophobic features (cyan spheres) and one acceptor feature (green sphere). The acceptor feature corresponds to the oxazole nitrogen, while the hydrophobic features correspond to the trifluoromethyl group on the phenyl ring and the methyl group on oxazole ring of the drug.

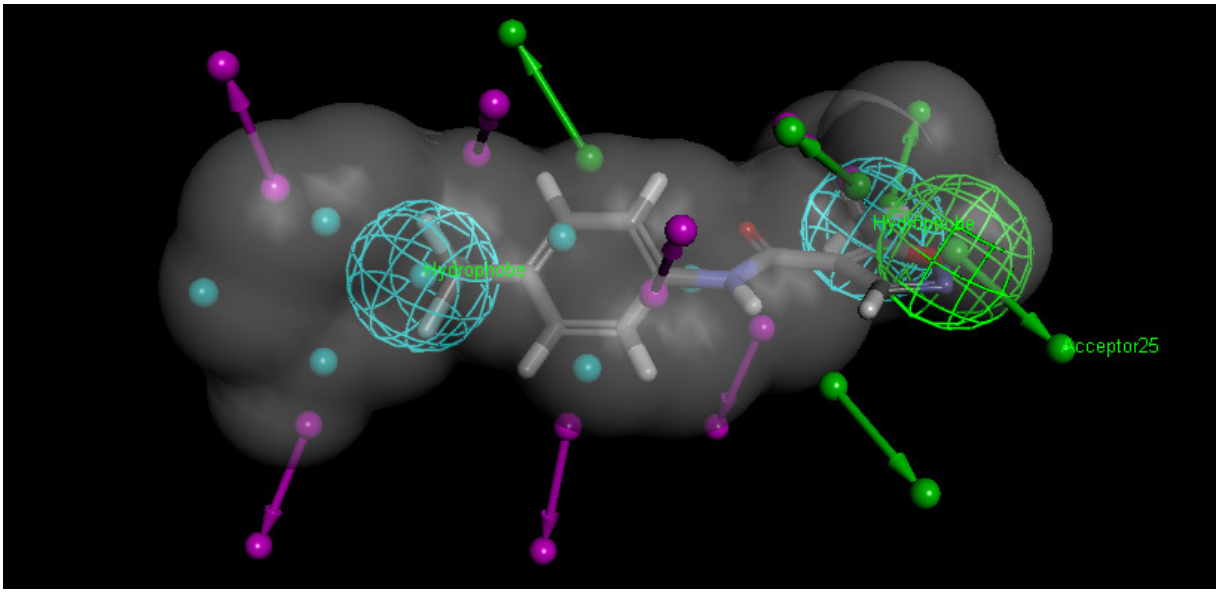

Figure 4.65. The orientation of leflunomide in the MAO-B structure-based pharmacophore model.

Although leflunomide is a relatively good MAO inhibitor, the interactions of leflunomide with the MAO-A and MAO-B enzymes were not further examined. As mentioned above, leflunomide is a prodrug and has a very short half-life in plasma. It is therefore not probable that leflunomide will be a significant inhibitor of MAO *in vivo* in humans. The structure of leflunomide may, however, serve as a lead for the design of future MAO inhibitors. This is worthy of further investigation in future studies.

4.5.9. Ondansetron

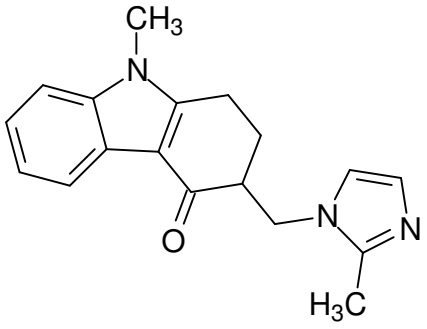

Figure 4.66. The structure of ondansetron.

The structure of ondansetron is given above. Ondansetron is a highly selective 5-HT_3 receptor antagonist. It has superior anti-emetic efficacy over metoclopramide in the prevention of nausea and vomiting induced by cisplatin, an anti-neoplastic drug (Fumoleau *et al*., 1997). The results of the MAO inhibition studies show that ondansetron is an inhibitor of MAO-A. Ondansetron is not an inhibitor of MAO-B, even at maximal tested concentration of 100 µM. The concentration-response curves of the MAO-A and MAO-B catalytic activities in presence of increasing concentrations of ondansetron are given below. The graph shows that there is no significant decrease in the catalytic activity of MAO-B with increasing concentrations of ondansetron. There is, however, a significant decrease in the catalytic activity of MAO-A with increasing concentrations of ondansetron. Maximal suppression of MAO-A activity was, however, not achieved with the maximal concentration tested 100 µM. The IC_{50} values recorded for the inhibition of MAO-A and MAO-B are estimated at 120.7 ± 28.6 µM and 188.4 ± 12.5 µM, respectively.

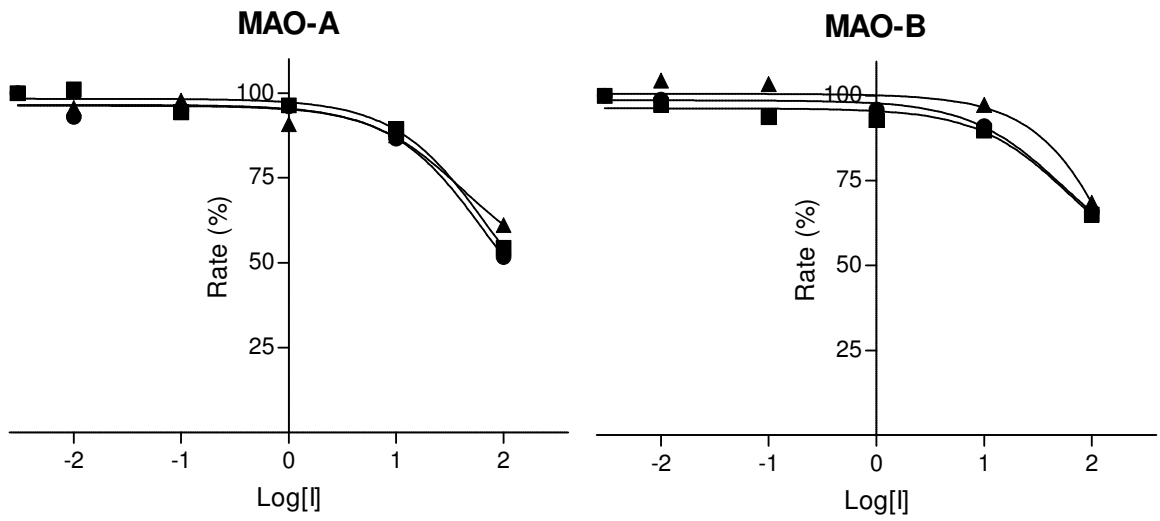

Figure 4.67. The recombinant human MAO-A (left) and MAO-B (right) catalyzed oxidation of kynuramine in the presence of various concentrations of ondansetron (expressed in µM). The concentration-response curves were constructed from the initial rates of kynuramine oxidation versus the logarithm of the concentration of ondansetron. The rates are expressed as the percentage of the catalytic rate recorded in the absence of inhibitor.

4.5.10. Pantoprazole

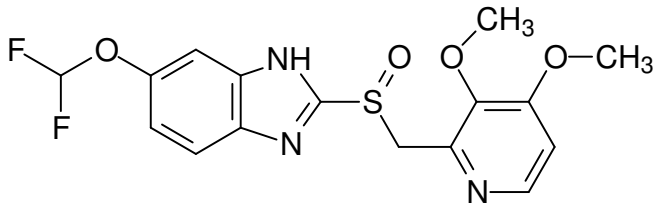

Figure 4.68. The structure of pantoprazole.

The structure of pantoprazole is given above. Pantoprazole is a proton pump inhibitor used in the treatment of erosive esophagitis associated with gastroesophageal reflux disease (Avner, 2000). The results of the MAO inhibition studies show that pantoprazole is an inhibitor of MAO-A. Pantoprazole is a very weak inhibitor of MAO-B, even at maximal tested concentration of 100 µM. The concentration-response curves of the

MAO-A and MAO-B catalytic activity in presence of increasing concentrations of pantoprazole are given below. The graph shows that there is only a small decrease in the catalytic activity of MAO-B with increasing concentrations of pantoprazole. There is however a slightly more significant decrease in the catalytic activity of MAO-A with increasing concentrations of pantoprazole. Maximal suppression of MAO-A activity was, however, not achieved with the maximal concentration tested 100 µM. The IC_{50} values recorded for the inhibition of MAO-A and MAO-B are estimated at 109.4 ± 4.8 µM and 201.7 ± 22.9 µM, respectively.

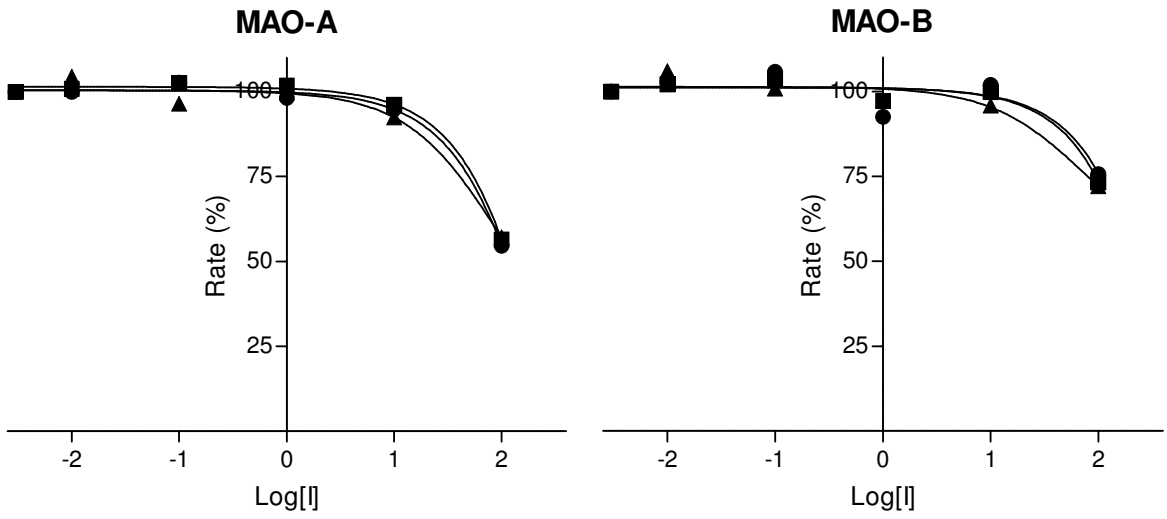

Figure 4.69. The recombinant human MAO-A (left) and MAO-B (right) catalyzed oxidation of kynuramine in the presence of various concentrations of pantoprazole (expressed in µM). The concentration-response curves were constructed from the initial rates of kynuramine oxidation versus the logarithm of the concentration of pantoprazole. The rates are expressed as the percentage of the catalytic rate recorded in the absence of inhibitor.

4.5.11. Tolcapone

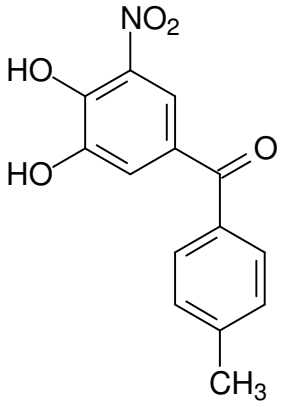

Figure 4.70. The structure of tolcapone.

The structure of tolcapone is given above. Tolcapone is a selective, reversible COMT inhibitor that stabilizes plasma levodopa concentrations and improves the "wearing off" period in patients on levodopa treatment (Agid *et al*., 1997). The results of the MAO inhibition studies show that tolcapone is an inhibitor of both MAO-A and MAO-B. The concentration-response curves of the MAO-A and MAO-B catalytic activities in presence of increasing concentrations of tolcapone are given below. The graph shows that there is a significant decrease in the catalytic activities of MAO-A and MAO-B with increasing concentrations of tolcapone. Maximal suppression of MAO-A and MAO-B activities were, however, not achieved with the maximal concentration tested 100 µM. The IC_{50} values recorded for the inhibition of MAO-A and MAO-B are estimated at 63.3 ± 10.8 µM and 53.4 ± 5.7 µM, respectively.

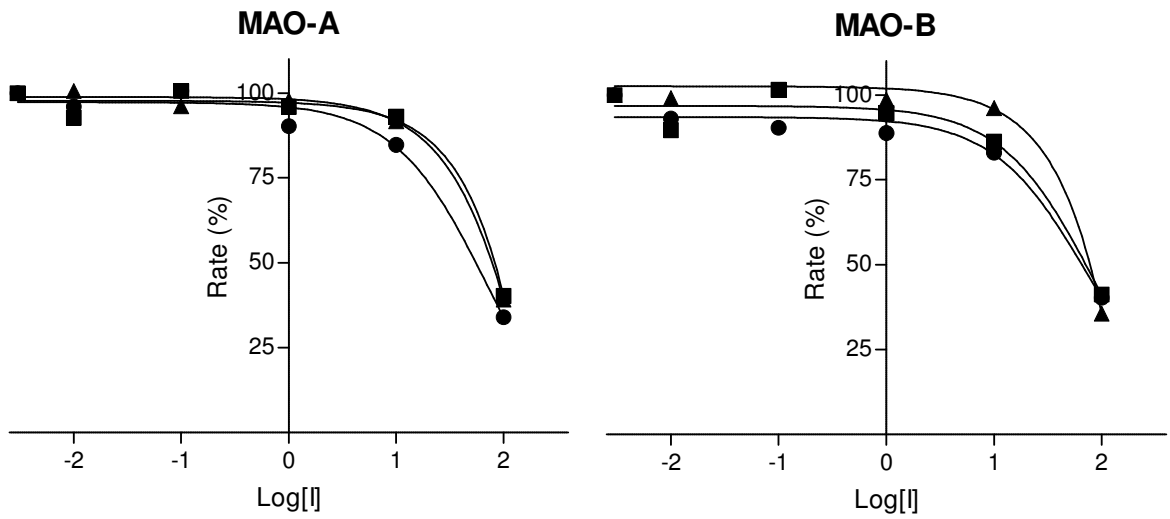

Figure 4.71. The recombinant human MAO-A (left) and MAO-B (right) catalyzed oxidation of kynuramine in the presence of various concentrations of tolcapone (expressed in µM). The concentration-response curves were constructed from the initial rates of kynuramine oxidation versus the logarithm of the concentration of tolcapone. The rates are expressed as the percentage of the catalytic rate recorded in the absence of inhibitor.

4.5.12. Tolmetin

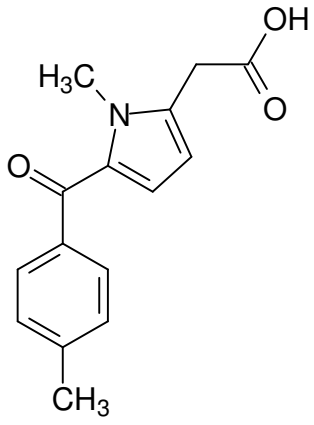

Figure 4.72. The structure of tolmetin.

The structure of tolmetin is given above. Tolmetin is a nonsteroidal anti-inflammatory agent used for pain, inflammation, arthritis and rheumatoid arthritis (Dairam *et al*., 2006). The results of the MAO inhibition studies show that tolmetin is an inhibitor of MAO-B. Tolmetin is a weak inhibitor of MAO-A, even at maximal tested concentration of 100 µM. The concentration-response curves of the MAO-A and MAO-B catalytic activity in presence of increasing concentrations of tolmetin are given below. The graph shows that there is only a small decrease in the catalytic activity of MAO-A with increasing concentrations of tolmetin. There is however a more significant decrease in the catalytic activity of MAO-B with increasing concentrations of tolmetin. Maximal suppression of MAO-B activity was, however, not achieved with the maximal concentration tested 100 µM. The IC_{50} values recorded for the inhibition of MAO-A and MAO-B are estimated at 129 ± 8.9 µM and 70.8 ± 3.3 µM, respectively.

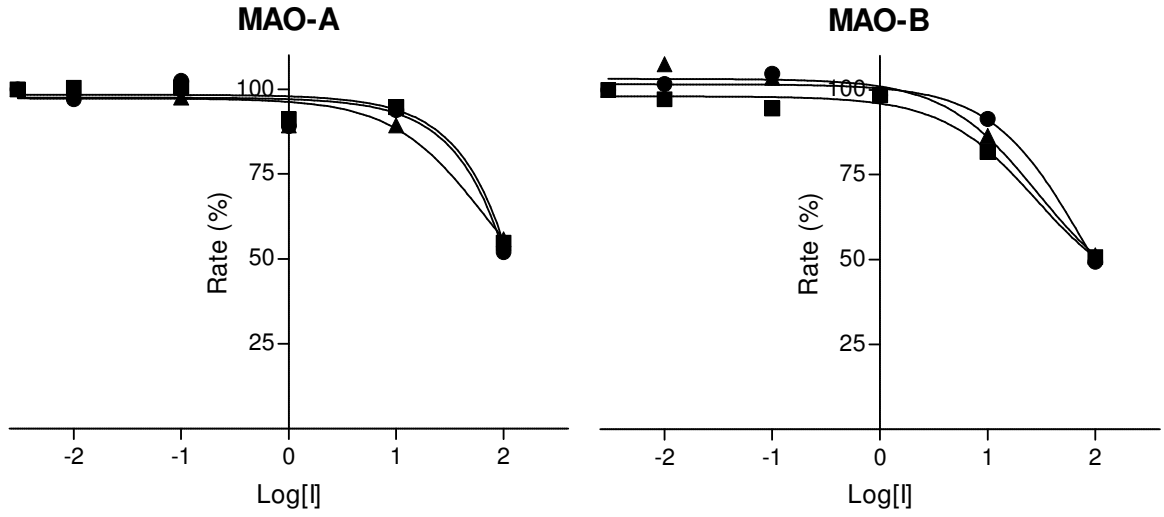

Figure 4.73. The recombinant human MAO-A (left) and MAO-B (right) catalyzed oxidation of kynuramine in the presence of various concentrations of tolmetin (expressed in µM). The concentration-response curves were constructed from the initial rates of kynuramine oxidation versus the logarithm of the concentration of tolmetin. The rates are expressed as the percentage of the catalytic rate recorded in the absence of inhibitor.

4.5.13. Tolnaftate

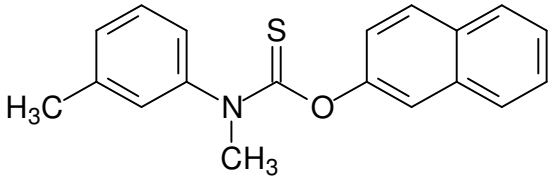

Figure 4.74. The structure of tolnaftate.

The structure of tolnaftate is given above. Tolnaftate is an anti-fungal for topical use. It is used in the prevention of mycosis hyperhidrosis in the form of a powder and the treatment of superficial mycoses as a spray (Czeizel *et al*., 2004). It may also be used in the treatment of fungal infections such as *Aspergillus fumigates, Aspergillus niger*, *Candida parapsilosis* and *Candida albicans* (Munguia & Daniel, 2008). The results of the MAO inhibition studies show that tolnaftate is an inhibitor of both MAO-A and MAO-B. The concentration-response curves of the MAO-A and MAO-B catalytic activity in presence of increasing concentrations of tolnaftate are given below. The graph shows that there is a significant decrease in the catalytic activities of MAO-A and MAO-B with increasing concentrations of tolnaftate. Maximal suppression of MAO-A and MAO-B activities were, however, not achieved with the maximal concentration tested 100 µM. The IC_{50} values recorded for the inhibition of MAO-A and MAO-B are estimated at 17.4 ± 2 µM and 8.1 ± 0.8 µM, respectively.

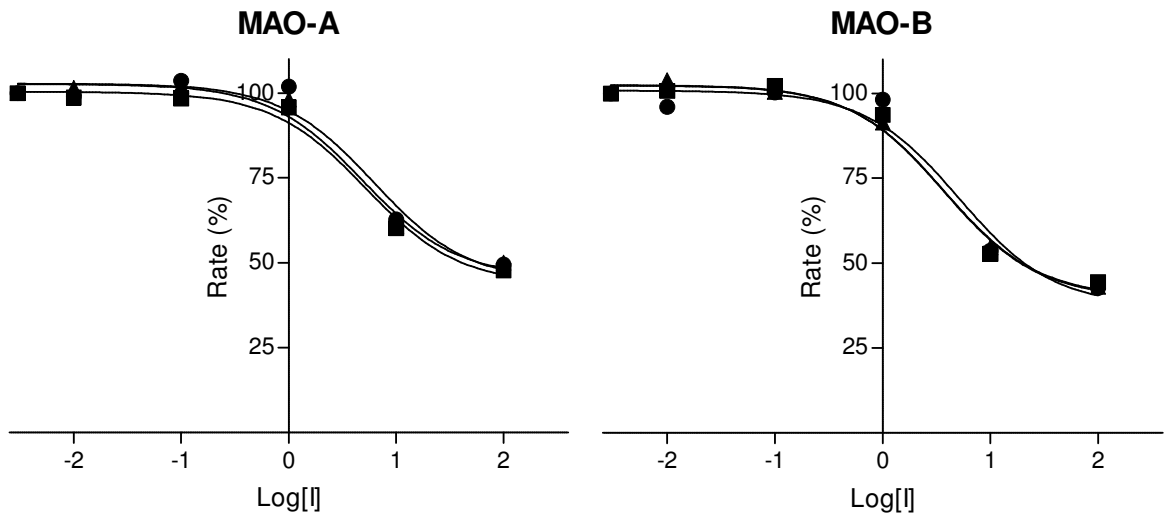

Figure 4.75. The recombinant human MAO-A (left) and MAO-B (right) catalyzed oxidation of kynuramine in the presence of various concentrations of tolnaftate (expressed in µM). The concentration-response curves were constructed from the initial rates of kynuramine oxidation versus the logarithm of the concentration of tolnaftate. The rates are expressed as the percentage of the catalytic rate recorded in the absence of inhibitor.

4.6. Results of the MAO inhibition studies with known MAO inhibitors.

In order to compare the MAO inhibition potencies of those drugs that were found to be active inhibitors with the inhibition potencies of known inhibitors, the IC_{50} values of known inhibitors were determined. The following inhibitors were selected:

- MAO-A inhibitor: Toloxatone
- MAO-B inhibitor: Lazabemide

These are both reversible MAO inhibitors.

4.6.1. Toloxatone

The results of the MAO-A inhibition studies show that toloxatone inhibits MAO-A with an IC_{50} value of 3.92 ± 0.015 µM. The literature value is 3.26 µM (Curet *et al*., 1998).

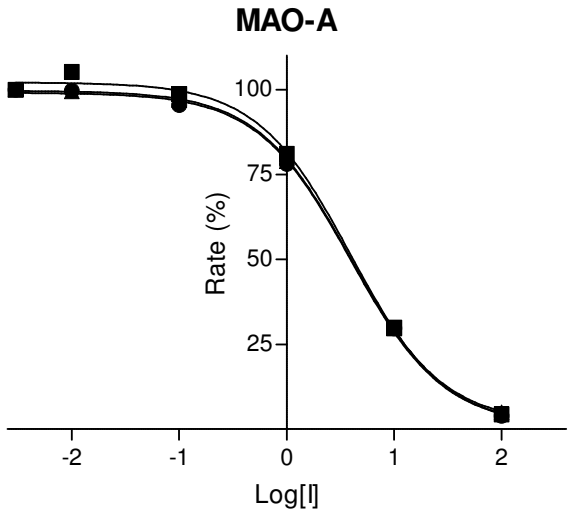

Figure 4.76. The recombinant human MAO-A catalyzed oxidation of kynuramine in the presence of various concentrations of toloxatone (expressed in µM). The concentration-response curves were constructed from the initial rates of kynuramine oxidation versus the logarithm of the concentration of toloxatone.

4.6.2. Lazabemide

The results of the MAO-B inhibition studies show that lazabemide inhibits MAO-B with an IC_{50} value of 0.091 ± 0.015 µM. The literature value is 0.03 µM (Curet *et al*., 1998).

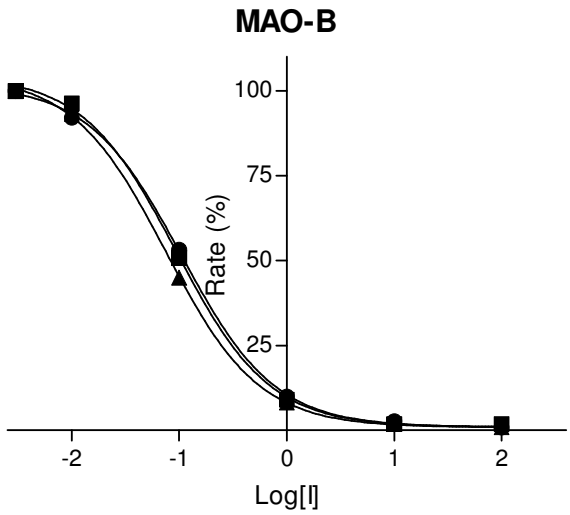

Figure 4.77. The recombinant human MAO-B catalyzed oxidation of kynuramine in the presence of various concentrations of lazabemide (expressed in µM). The concentration-response curves were constructed from the initial rates of kynuramine oxidation versus the logarithm of the concentration of lazabemide.

4.7. Summary

In this chapter, the *in vitro* studies showed that 16 of the compounds that mapped to the structure-based pharmacophore model had no inhibitory activity towards MAO-A or MAO-B. However, there were 4 of the compounds which showed a small amount of inhibitory activity at 100 µM towards one or both of the isoforms of the MAO-enzyme. This may not be of any significance, as the inhibitory activity was shown in only one replicate of the triplicate determinations. The compounds may have the required features to map to the MAO-enzymes, but do not possess strong inhibitory activity *in vitro*. This suggests that different approaches may be needed in the pharmacophore development and screening. These approaches include the use of exclusion constraints instead of shape constraints and making certain features a requirement for compounds to be considered hits. Furthermore the MAO-enzymes have a broad inhibitory specificity and a wide variety of drugs may thus map to the MAO pharmacophores, but may not necessarily inhibit the enzyme *in vitro* in a significant way.

The *in vitro* studies showed that 13 of the compounds that mapped to the structure-based pharmacophore models had inhibitory activity towards MAO-A and/or MAO-B. Of these 13 compounds, 3 were investigated further. These compounds include caffeine, esomeprazole and leflunomide. Esomeprazole and caffeine was found to be reversible inhibitors, which is important in the prevention of unwanted side effects such as the cheese reaction. Although caffeine possesses a relatively weak MAO inhibitory effect, it is a reversible, competitive inhibitor of MAO-B and MAO-A. Esomeprazole proved to be a good inhibitor, especially towards MAO-A. The *in vitro* studies show that esomeprazole is a reversible, competitive inhibitor of MAO. Leflunomide has good inhibitory activity toward MAO. Leflunomide is, however, a prodrug with a very short half-life in plasma and therefore it may not be a significant inhibitor of MAO *in vivo*. The results suggest that it is possible to discover new drugs with MAO-inhibitory potencies by screening a virtual library of existing drugs with the use of a structure-based pharmacophore model. The inhibitory potencies of many of these drugs may not be significant enough to repurpose them for the treatment of diseases such as Parkinson's disease, but structures such as leflunomide may serve as leads for the design of future MAO inhibitors.